Gliding arc plasma for CO_2 conversion: better insights by a combined experimental and modelling approach

Weizong Wang*[,1], Danhua Mei[2], Xin Tu[2] and Annemie Bogaerts[1]

1. Research group PLASMANT, Department of Chemistry, University of Antwerp, Universiteitsplein 1, B-2610 Wilrijk-Antwerp, Belgium

2. Department of Electrical Engineering and Electronics, University of Liverpool, Brownlow Hill, Liverpool L69 3GJ, United Kingdom

E-mail: wangweizong@gmail.com, Xin.Tu@liverpool.ac.uk, annemie.bogaerts@uantwerpen.be

Highlights

- A two dimensional self-consistent model is developed and validated by the direct experiment.

- Gliding arc shows a strong non-equilibrium character of the conversion process, explaining the higher values of conversion and energy efficiency than thermal process.

- A chemical kinetics analysis shows that the CO_2 vibrational levels significantly contribute to the CO_2 dissociation.

- Promoting the vibrational kinetics, reducing the recombination of CO with O_2 and increasing the CO_2 fraction treated by the arc can further improve the conversion and energy efficiency.

Abstract

A gliding arc plasma is a potential way to convert CO_2 into CO and O_2, due to its non-equilibrium character, but little is known about the underlying mechanisms. In this paper, a self-consistent two-dimensional (2D) gliding arc model is developed, with a detailed non-equilibrium CO_2 plasma chemistry, and validated with experiments. Our calculated values of the electron number density in the plasma, the CO_2 conversion and energy efficiency show reasonable agreement with the experiments, indicating that the model can provide a realistic picture of the plasma chemistry. Comparison of the results with classical thermal conversion, as well as other plasma-based technologies for CO_2 conversion reported in literature, demonstrates the non-equilibrium character of the gliding arc, and indicates that the gliding arc is a promising plasma reactor for CO_2 conversion. However, some process modifications should be exploited to further improve its performance. As the model provides a realistic picture of the plasma behaviour, we use it first to investigate the plasma characteristics in a whole gliding arc cycle, which is necessary to understand the underlying mechanisms. Subsequently, we perform a chemical kinetics analysis, to investigate the different pathways for CO_2 loss and formation. Based on the revealed discharge properties and the underlying CO_2 plasma chemistry, the model allows us to propose solutions on how to further improve the CO_2 conversion and energy efficiency by a gliding arc plasma.

Keywords: CO_2 conversion, gliding arc, non-equilibrium plasma, plasma chemistry, splitting mechanisms, breakdown

1. Introduction

Plasma technology offers unique perspectives, because of its capacity to induce chemical reactions within gases at ambient temperature and pressure, due to its non-equilibrium character. Plasma is created by applying electric power to a gas, causing breakdown of the gas into ions and electrons and also producing a large number of reactive species, such as various radicals and excited species. This makes plasma a highly reactive cocktail, which is quite promising for greenhouse gas conversion. Indeed, the inert CO_2 gas is activated by electron impact ionization, excitation and dissociation. Furthermore, plasma is very flexible and can easily be switched on and off, so it is quite promising for storing peak renewable energy into fuels. Indeed, more and more electrical energy nowadays is produced from renewable energy sources (wind or solar), which often suffer from fluctuating peak powers, making it difficult to match the supply of this electricity with the demand. This surplus of electricity can in principle be used in plasma to convert greenhouse gases into value added chemicals when adding a suitable H-source to the CO_2 gas, such as H_2O, CH_4 or H_2. However, there is still a long way to go, certainly if we target the selective production of some value-added products, for which the combination with a suitable catalyst would be needed. This makes plasma based greenhouse gas conversion fit in principle in the framework of green chemistry [1]-[2] and also complies with the "cradle-to-cradle" principle [3].

Gliding arc (GA) plasmas are potential plasma sources for gas conversion [4]-[18] because they offer benefits of both thermal and non-thermal discharges. They are typically considered as 'warm' discharges, which are characterized by a better energy efficiency than other types of plasmas. The reason is that they provide efficient vibrational excitation of the molecules, which is seen as the most energy-efficient way to split CO_2 molecules [19].

In order to improve the applications (i.e., mainly gas conversion), the physical and chemical characteristics of the GA have been extensively studied by experiments, including high-speed photography [20], electrical measurements [21]-[23] and spectroscopic measurements [24]-[25]. Besides experiments, detailed modelling is also very useful to provide more insight into the underlying reaction mechanisms of plasma assisted gas conversion or synthesis, not only in a GA but also in other types of plasmas. For example, computer modeling is widely used to evaluate quantities which are difficult to measure, and to identify the most important chemical reactions [26]-[32]. However, only a few papers in literature deal with modelling of a GA, typically applying a 1D analytical model, such as the Elenbaas–Heller model [33] or the plasma string model [34] without a detailed description of the chemical reactions occurring in the GA. Recently, a 2D non-quasi-neutral model was presented to study the arc root movement in an argon GA [35]-[36]. Moreover, 3D quasi-neutral models for a novel type of GA plasmatron [37] and a classical diverging electrode GA reactor [38]-[39] were also reported. However, these models were all developed for argon. For a GA operating in CO_2, the large number of species and related chemical reactions makes spatially resolved models computationally expensive. That is why only a limited number of numerical studies were reported so far on this subject, with only two papers for GA based CO_2 conversion published to

It is clear that more research is needed to fully exploit the capabilities of the GA for CO_2 conversion. In this paper, we therefore present a combined modeling and experimental study, based – for the first time – on a 2D model. The aim of this study is not only to elucidate the underlying mechanisms, but also – based on the obtained insights – to propose solutions on how to further improve the performance of the GA for CO_2 conversion.
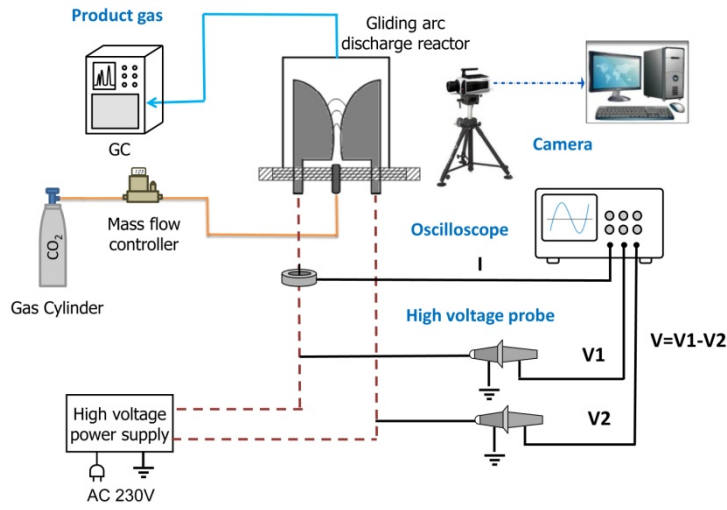
2. Experimental setup of the GA reactor

Figure 1 Schematic diagram of the GA experimental set-up

Figure 1 illustrates the experimental setup of the GA and surrounding measurement equipment. The GA reactor consists of two stainless steel semi-ellipsoidal electrodes with thickness of 2 mm (60 mm long and 18 mm wide) fixed in an insulating bracket and symmetrically placed on both sides of a gas nozzle with a diameter of 1.5 mm. The reactor is designed to facilitate easy electrode replacement, and the discharge gap between both electrodes, as well as the distance between the nozzle exit and electrode throat, is adjustable. Pure CO_2 gas was injected into the GA reactor and it pushes the arc plasma, which is initiated at the shortest gap between both electrodes, towards larger interelectrode distance until it extinguishes, and a new arc is created at the shortest gap. The plasma reactor was connected to a neon transformer (SIET, 230 V/10 kV, 50 Hz). The arc voltage was measured by a high voltage probe (Testec, TT-HVP 15 HF), while the arc current was recorded by a current monitor (Magnelab, CT-E 0.5-BNC). All the electrical signals were sampled by a four-channel digital oscilloscope (Tektronix, MDO 3024). The arc dynamics are revealed by means of a digital high-speed camera (Phantom V.7.1) which can record up to 4,800 pictures per second using the full 800x600 pixel SR-CMOS imaging sensor array. The measurement technique was intensely optimized to fine-tune the best recording conditions. The frame rates to visualize the arc propagation and the exposure time of the detector to enhance the contrast between the arc and the reactor were investigated. The products of the CO_2 conversion after passing through the GA reactor were sampled when the plasma reaction has reached a stable condition, i.e., typically after 30 min. The gaseous products were analyzed by a gas chromatograph (Shimadzu, GC-2014) equipped with a thermal conductivity detector (TCD) and a flame ionization detector (FID). As we mention below, a standard case of 2.5 L/min and 40W is used to validate our model. Furthermore, the vertical distance between the nozzle exit and electrode throat was 2 mm and the shortest discharge gap between the two electrodes was also 2 mm.

The plasma power is calculated by integration of the arc voltage and current, as shown in Eq. (1).

$$P_{plasma} = 1/T \int_0^{t=T} V_{plasma} \times I_{plasma} dt \qquad (1)$$

The conversion of CO_2, X_{CO_2}, is defined as:

1    $$X_{CO_2}(\%) = \frac{CO_{2(in)} - CO_{2(out)}}{CO_{2(in)}} \times 100\% \qquad\qquad (2)$$

2   where $CO_{2(in)}$ and $CO_{2(out)}$ are the CO$_2$ signals without and with plasma, respectively. Since the method

3   mentioned above does not account for the gas expansion due to CO$_2$ splitting, a correction factor is

4   used, which is explained in the supplementary information of Ref [31].

5   In order to calculate the energy efficiency of CO$_2$ conversion, the specific energy input (SEI) in

6   the plasma is defined as:

7    $$SEI\left(\frac{kJ}{L}\right) = \frac{Plasma\ power\ (kW)}{Flow\ rate\ (\frac{Ln}{min})} \times 60\left(\frac{s}{min}\right) \qquad\qquad (3)$$

8   where the flow rate is expressed in L$_n$/min (liters normal per minute) with reference conditions at a

9   temperature of 0 °C and a pressure of 1 atm.

10   The energy efficiency, η, is calculated as:

11   $$\eta(\%) = \frac{\Delta H_R\left(\frac{kJ}{mol}\right) \times X_{CO_2}(\%)}{SEI\left(\frac{kJ}{L}\right) \times 22.4\left(\frac{L}{mol}\right)} \qquad\qquad (4)$$

12   where ΔH_R is the reaction enthalpy of CO$_2$ splitting (i.e., 279.8 kJ/mol), X_{CO_2} is the amount of CO$_2$

13   converted, SEI is defined above and 22.4 L/mol is the molar volume at 0 °C and 1 atm.

14   The experiments were performed 4 times and they were reproducible within +/- 5% of the

15   averaged values.

16   **3. Description of the 2D plasma slab model**

17   **3.1 The GA reactor geometry**

18
19   (a)   (b)
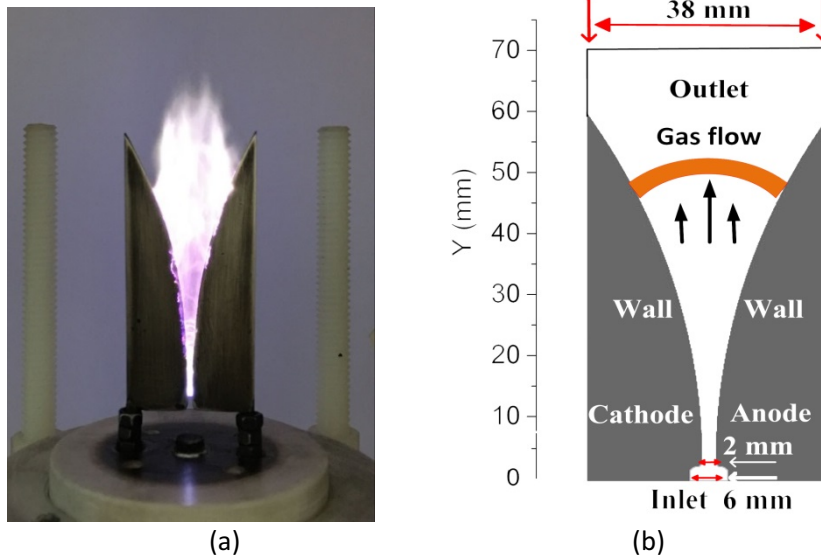

20   Figure 2 Photograph of the GA reactor (a) and schematic illustration of the geometry considered in

21   the model (b).

22   The 2D fluid model that we developed applies to a Cartesian geometry, which allows to describe

23   the gliding of a '2D arc', which is basically a finite plasma slab. The simulated geometry in the

24   direction perpendicular to the simulation plane is assumed to be equal to the electrode thickness of

25   2 mm. Hence, the electrical current in the 2D model is obtained by integration of the current density

4

1 over the arc slab, which fits the experimental signal. Furthermore, the flow field is determined by
2 taking into account a flow passing channel with a depth of 2 mm with the specified flow rate. In this
3 way, the calculated gas velocity is similar to the experimental data when the vertical distance
4 between the nozzle exit and electrode throat was 2 mm and the shortest discharge gap between the
5 two electrodes was also 2 mm. Indeed, a rough estimation of the experimental gas velocity is
6 obtained by examination of the arc displacement shown in successive high-speed photographs (see
7 supporting information). In principle, a 3D model would be required to describe the GA behaviour in
8 a realistic way, in view of the intrinsic 3D nature of the GA. However, a 3D model is very time
9 consuming and it requires significant computer resources, especially when modelling a CO_2 plasma
10 with complicated plasma chemistry. Furthermore, previous work for an argon GA [38] has shown
11 that the results of a 2D model compare well with those of a 3D model, and can thus be used for a
12 better understanding of the GA basic characteristics. The total width and height of the model
13 geometry, including the region outside the electrodes where the gas can flow without passing
14 through the arc, is 38 mm and 70 mm, respectively.

15 **3.2 CO_2 plasma chemistry and treatment of the vibrational levels**

16 The chemistry set is based on the full chemistry set developed by Kozák and Bogaerts [26]-[27]
17 with a 0D model, but reduced to include only the most important species and processes. In this way,
18 we can avoid excessive calculation times in this 2D model, but we still account for the vibrational
19 kinetics, which is crucial for describing CO_2 conversion in a GA plasma reactor [41]. The list of species
20 considered in the model is shown in table 1. These species include various neutral molecules in the
21 ground state, as well as in various electronically and vibrationally excited levels, a number of radicals,
22 positive and negative ions, and the electrons. In the full model of Kozák and Bogaerts [26]-[27], 25
23 CO_2 vibrational levels (i.e., 4 effective levels of the symmetric modes and 21 levels of the asymmetric
24 stretch mode, up to the dissociation limit) were taken into account. However, to further reduce the
25 calculation time, which is needed to implement this chemistry in a 2D model, Berthelot and Bogaerts
26 [42] developed a level lumping method, which groups the 21 asymmetric stretch mode vibrational
27 levels into a number of lumped levels, without loss of essential information. We applied this level
28 lumping method in [41] for a 1D gliding arc model, and we illustrated that lumping the 21 levels into
29 3 groups can reproduce the plasma properties, the vibrational distribution function (VDF) and the
30 CO_2 conversion very well. Therefore, we adopt here the same level lumping method with 3 groups
31 for the asymmetric stretch mode, with each group including 7 vibrational levels (group 1: $CO_2[v_1\text{-}v_7]$,
32 group 2: $CO_2[v_8\text{-}v_{14}]$, group 3: $CO_2[v_{15}\text{-}v_{21}]$). The species number density of each level within one
33 group can be determined following the method described in [41-42]. Besides, we also take into
34 account the 4 effective levels of the symmetric modes ($CO_2[v_a] - CO_2[v_d]$), 1 electronically excited
35 level of CO_2 ($CO_2[e]$), and 3 vibrational levels of O_2 ($O_2[v1] - O_2[v3]$), as indicated in table 1.

36 Table 1 Overview of the plasma species included in the model.

Neutral ground state species	CO_2, CO, C, O_2, O
Neutral excited states	$CO_2[v_a]$, $CO_2[v_b]$, $CO_2[v_c]$, $CO_2[v_d]$, $CO_2(v_1\text{-}v_7)$, $CO_2(v_8\text{-}v_{14})$, $CO_2(v_{15}\text{-}v_{21})$, $CO_2[e]$, $O_2[v1]$, $O_2[v2]$, $O_2[v3]$
Charged species	CO_2^+, O_2^+, CO_3^-, O^-, O_2^-, e^-

37 All these species undergo a large number of chemical reactions, i.e., electron impact collisions
38 with neutral species, leading to excitation, ionization, dissociation and electron attachment,

electron–ion recombination reactions, as well as many heavy-particle chemical reactions (i.e., ion-ion, ion-neutral and neutral-neutral reactions). We pay special attention to the reactions of the vibrational levels, i.e., electron impact vibrational excitation, and vibrational energy exchange upon collision with ground state species or other vibrationally excited levels (i.e., so-called vibrational-translational (VT) and vibrational-vibrational (VV) relaxation, respectively). Moreover, the same chemical reactions as for the ground state species are carefully included for the vibrational levels as well, because the vibrational energy can help overcome the activation energy barrier of the reactions and thus increase the reaction rate of CO_2 splitting. The chemical reactions, the corresponding rate coefficients and the references where these data were adopted from, are listed in our previous work [41].

3.3 System of governing equations and boundary conditions

The model calculates the densities of all the plasma species, the electron temperature and gas temperature and the electric field in the GA, as well as the gas flow profile. We assume electrical neutrality in the plasma, because the sheath is not considered in our model. This assumption has no significant influence on the arc column [39]. The species densities and the electron mean energy are calculated with continuity equations based on transport and on production and loss terms defined by the chemical reactions (and by Joule heating for the electron energy). The species transport is based on drift in the electric field and diffusion due to concentration gradients. As we assume electrical neutrality in the arc plasma, the ambipolar electric field is calculated from the charged species densities. The gas heat transfer equation is solved for the gas translational temperature, and finally, the neutral gas flow, which is responsible for the arc displacement, is described by the Navier-Stokes equations, providing a solution for the mass density and the mass-averaged velocity. The Navier-Stokes equations are first solved separately, and subsequently, the obtained velocity distribution is used as input data in the other equations, describing the plasma behavior and the gas heating. The equations solved, as well as the corresponding boundary conditions, are explained in detail in the supporting information. Finally, the external circuit and the power supply need to be specified in the simulation. The source voltage has a sinus shape, V_{source} = 7200sin (2π50t + 0.50) V, and a resistance of 60 kΩ is used to limit the discharge current; it provides a total arc discharge power of 40 W, which is similar to the typical experimental value at a gas flow rate of 2.5 L/min.

The equations are solved by means of the COMSOL Multiphysics software [43], a commercial finite element software designed for solving problems of multi-physics. As initial values we assume that the concentrations of CO_2 in the ground state and in the various excited levels follow a Maxwellian distribution at room temperature.

4. Results and discussion

In section 4.1 we will first validate our model by comparing our calculated values with experimental data for the electron number density (which is one of the most important plasma properties), as well as for the CO_2 conversion and corresponding energy efficiency. Subsequently, in section 4.2 we will benchmark our results for the CO_2 conversion and energy efficiency to the classical thermal conversion process and to other plasma-based technologies for CO_2 conversion reported in literature. This allows us to provide a clear overview of the capabilities of the GA for CO_2 conversion, as well as its limitations, for which we should propose some process modifications, to further improve the results. In order to achieve this, we need a better insight in the typical discharge characteristics, as calculated by the model, which will be presented in section 4.3. Furthermore, we

1 will also perform a chemical kinetics analysis in section 4.4, to elucidate the role of various plasma
2 species and their reactions in the GA based CO_2 conversion. Finally, based on the revealed discharge
3 properties and the obtained plasma chemistry, we will propose in section 4.5 some solutions on how
4 to further improve the CO_2 conversion and the energy efficiency by the GA.

4.1 Experimental validation of the model

6   Table 2 Comparison of our calculated values for electron number density, CO_2 conversion and
7 energy efficiency, with the experimental data, at a gas flow rate of 2.5 L/min and a discharge power
8 of 40 W.

Results	Electron number density	Conversion	Energy efficiency
Calculation	10^{18}-10^{19} m^{-3}	2.78 %	32.8 %
Experiment	2.6×10^{18} m^{-3}	2.90 %	34.3 %
Experimental error	4.9%	4.3%	4.6%

9   In table 2 we compare our calculated results for the electron number density, CO_2 conversion
10 and corresponding energy efficiency with the corresponding measured values, at a typical
11 experimental gas flow rate of 2.5 L/min and a discharge power of 40 W.

12   The experimental electron number density is obtained from the electrical characteristics and the
13 high speed camera images, as follows. During the propagating phase of the GA, the average
14 experimental voltage drop across the arcs is V ≈ 1.20 kV with an average current of I ≈ 0.06 A (see
15 figure S1 of the supporting information), leading to an average arc impedance <R> = V/I ≈ 20 kΩ. The
16 radius of the arc (λ ≈ 1 mm) and the average length (<w> ≈ 15 mm) are obtained by the high speed
17 camera recordings (see figure S2 of the supporting information). With this information, we can
18 calculate the average arc electrical conductivity, σ, as

19 $$\sigma = \frac{\langle w \rangle}{<R>\pi\lambda^2}$$ (5)

20 yielding σ ≈ 0.24 S/m. The conductivity can be related to the electron density through the electron
21 mobility, μ_e, using:

22 $$< n_e > = \frac{\sigma}{e\mu_e}$$ (6)

23 With e the electron charge. Using a time averaged gas temperature of 2400 K and an electron
24 temperature of 1.7 eV, as obtained from our model (see section 4.3), we calculated $\mu_e =$
25 $0.56\ m^2/V/S$ by means of a Boltzmann equation solver BOLSIG+ [44]. Hence, formula (6) gives an
26 estimate of the time and spatially averaged electron number density, $<n_e> \approx 2.6 \times 10^{18}$ m^{-3}. Our
27 calculations predict the maximum electron number density in the discharge channel to be around
28 10^{19} m^{-3} (see section 4.3). Considering the non-uniform distribution within the discharge channel, we
29 can obtain a spatially averaged value of the electron number density within the range 10^{18} m^{-3}-10^{19}
30 m^{-3}, indicating a reasonable agreement between the calculated and measured values.

31   The calculated conversion of CO_2, $X_{CO_2}^C$, is determined as:

32 $$X_{CO_2}^C = \frac{\int r_{CO_2} dV \int dt}{\int Q_{co2(in)} dt} \times 100\% = \frac{l_0 \int r_{CO_2} dS \int dt}{\int Q_{co2(in)} dt} \times 100\%$$ (7)

1 where $Q_{co_2(in)}$ is the particle flow rate of CO_2 entering the reactor per second (in s^{-1}), r_{CO_2} is the net
2 splitting rate of CO_2 inside the arc (in m^{-3}s^{-1}), and l_0 = 2 mm, is the thickness of the GA reactor (see
3 below).

4 The particle flow rate of CO_2, $Q_{co_2(in)}$, represents the total number of CO_2 molecules flowing
5 into the reactor per second, and is obtained as follows:

$$Q_{co_2(in)}\left(\frac{1}{s}\right) = \frac{Q_n(\frac{L_n}{min})\times 0.001(\frac{m^3}{L_n})\times\frac{1}{60}(\frac{min}{s})\times P_0(Pa)}{k(\frac{J}{K})\times T_0(K)}\times 100\% \qquad (8)$$

7 where k is the Boltzmann constant, Q_n is the gas flow rate at the standard temperature T_0 = 273 K
8 and pressure P_0 =101325 Pa.

9 The net splitting rate of CO_2, r_{CO_2} in m^{-3}s^{-1}, represents the net number of dissociated CO_2
10 molecules per volume and per second, and is obtained by taking into account all the chemical
11 reactions, leading to destruction (when a positive value) or formation (when negative) of CO_2
12 molecules. In order to determine the total conversion of CO_2, as shown in equation (6), the net
13 splitting rate of CO_2, r_{CO_2}, is integrated spatially over the whole reactor and temporally over the
14 whole gliding cycle. Because of the prohibitively long computation time in a 3D model, a 2D plasma
15 slab model is used, assuming that the distribution of plasma parameters in the direction
16 perpendicular to the simulation plane (see figure 2b) is uniform. As a result, the arc is not a "wire"
17 but a "slab" with a length l_0 in the direction perpendicular to the simulation plane. We assume l_0 is
18 equal to the thickness of the GA reactor, i.e., 2 mm. Thus the total conversion of CO_2 in the 2D model
19 is obtained by the integration of the net splitting rate of CO_2 r_{CO_2} over the arc slab with l_0 = 2 mm.

20 Our calculated conversion and energy efficiency of CO_2, at a gas flow rate of 2.5 L/min and a
21 discharge power of 40 W, are 2.78 % and 32.8 %, respectively, which is also in satisfactory agreement
22 with the experimental values of 2.90 % and 34.3 %. The comparison of these three key parameters
23 indicates that our model most probably can provide a realistic picture of the plasma chemistry.

24 Comparison of other plasma characteristics, such as the electron temperature or gas
25 temperature, was not possible, as the latter properties could not be determined in our experimental
26 setup, and are also not available in literature for a pure CO_2 GA. This is probably because optical
27 emission spectrometry is not suitable here, as there are no proper spectral lines that can be used.
28 However, our calculated values for electron temperature (up to 1.7 eV) and gas temperature (up to
29 around 2700 K) are comparable with experimental data from literature, for GA reactors using other
30 molecular gases (nitrogen and air) [45]-[47], as well as for gaseous mixtures containing CO_2 [48]- [49].
31 For example, Wu et al. [48] measured values for the electron excitation temperature of
32 approximately 1.1-1.7 eV, using a rotating GA reactor for a mixture of CH_4/CO_2. Moreover, in a non-
33 equilibrium GA "tornado" discharge using CO_2 doped with 1% N_2, the rotational gas temperature was
34 determined to be 2700K ± 50 K [49].

35 We can only compare here the calculated and experimental data at a gas flow rate of 2.5 L/min
36 and discharge power of 40 W, because at these conditions the arc was observed to glide smoothly
37 along the electrodes. Indeed, at higher gas flow rates, a phenomenon of back-breakdown occurs,
38 affecting the arc gliding process (see further). These back-breakdown events cannot self-consistently
39 be captured by the model, because this behaviour is mostly stochastic by nature and the arc
40 instabilities are not well defined. Therefore, we would need to make some assumptions in the model

on the number of back-breakdown events, and depending on the values assumed for the back-breakdown frequency, we would always be able to obtain good agreement with the experiments. Hence, we lose the real validation possibility at higher gas flow rates. Therefore, we could only validate the model at a gas flow rate of 2.5 L/min and a discharge power of 40 W, where our high speed camera did not record any back-breakdown events. However, in section 4.5, we will assess the effect of a different number of back-breakdown events on the calculated conversion and energy efficiency, which can in principle be correlated with different values of gas flow rate and discharge power.

4.2 Comparison of our results with other plasma systems from literature
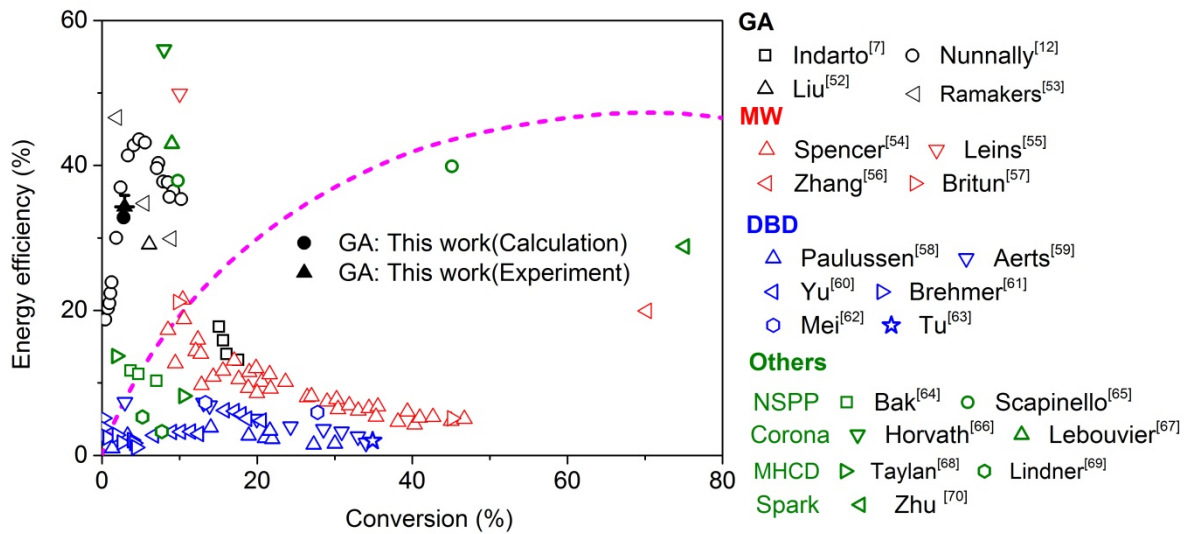
Figure 3 Energy efficiency vs CO_2 conversion, obtained in our experiments and calculations (black solid symbols), and comparison with other GA results from literature (black open symbols), as well as with results from other types of plasma reactors used for CO_2 conversion, operating at atmospheric pressure. The thermal conversion limit is also indicated.

In figure 3, we compare our results for the energy efficiency vs CO_2 conversion with data obtained from literature for CO_2 splitting, in other GA discharges[5],[6],[50],**Error! Reference source not found.**, as well as in other types of plasma reactors, such as microwave (MW) plasma [51]-[55], dielectric barrier discharge (DBD) [56]-[61], nano-second pulsed plasma (NSPP) [62]-[63], corona discharge [64]-[65], micro hollow cathode discharge (MHCD) [66]-[67] and spark discharge [68]. We can conclude that in terms of energy efficiency, the GA plasma is very promising, similar to the corona discharge [64]-[65]. It should be mentioned that for MW plasmas some higher energy efficiencies (i.e., up to 80 and 90%) were obtained in literature by Rusanov et al.[69] and Asisov et al.[70], respectively. However, their MW plasma reactors were operating at a reduced pressure of 0.06 - 0.26 atm and 0.05 – 0.2 atm, respectively, and thus they need vacuum equipment. This makes it more difficult to be applied on industrial scale, and the energy cost of the pumping system should also be included when calculating the energy consumption. Bongers et al. recently obtained values up to 50%, when applying a reverse vortex gas flow [73], but again these experiments were conducted at reduced pressures of 150 – 600 mbar (0.15 – 0.60 atm). In order to allow a fair comparison, we therefore only present results in figure 3, obtained at atmospheric pressure. When the MW discharge is operating at atmospheric pressure, the reported energy efficiency dramatically drops to values of about 5 - 20 % [51]-[55].

If we compare our results with those obtained in other GA reactors from literature, it is important to explain that there exist roughly two different reactor designs. The classical GA reactor, which is used in this study, typically consists of two plane diverging electrodes between which the gas flows. In contrast, recently a three-dimensional GA reactor, consisting of cylindrical electrodes with tangential gas inlet, leading to a vortex gas flow configuration, has been developed, also called GA plasmatron (GAP) [19]. Indarto et al. [5] applied a classical GA configuration, like in our case, and they obtained a highest energy efficiency of around 17%, which is much lower than our current work. On the other hand, Nunnally et al. [6], Liu et al. [50] and Ramakers et al. **Error! Reference source not found.** used a vortex flow GAP, which can reach a somewhat higher conversion and energy efficiency. This reactor design is indeed very promising, because it can be more easily implemented in industry and the specific gas flow configuration ensures the gas treatment to be more uniform. This indicates that a better design of the classical GA reactor, to enhance the treated gas volume, would improve the conversion performance, as will be discussed in detail in section 4.5 below. However, in general we can deduce from figure 3 that the GA plasma shows a very good performance with a relatively high energy efficiency. This is because the energy efficient vibrational excitation processes are favoured, as will be revealed in section 4.4 below.

It is obvious from figure 3 that a DBD plasma [56]-[61] has a reasonable conversion but a quite low energy efficiency. This is due to the non-ideal operating conditions, as the electron temperature is typically higher than in a GA (or MW) plasma [19],[72], and the mechanism of CO_2 conversion involves charged and electronically excited species, and thus it is limited by the high energy cost for the formation of these species. The same applies for the nano-second pulsed plasma (NSPP) [62]-[63] which also has a rather low energy efficiency. The process capability of the micro hollow cathode discharge (MHCD) [66]-[67] is very limited due to its very small volume. Therefore, it generally also exhibits a relatively low energy efficiency. The spark discharge [68] has a very high conversion, because of the very high energy consumption. The energy efficiency is also quite high, but it is lower than the thermal conversion process. This may be attributed to the fact that most of the energy is spent on the gas heating and the energy exchange with the surroundings. In general, we can conclude that the energy efficiency in our GA reactor at atmospheric pressure is better than the DBD plasma, microwave plasma, nano-second pulsed plasma and micro hollow cathode discharge plasma, and comparable to the corona discharge [64]-[65].

Finally, we also benchmark our results for the GA based CO_2 conversion to the pure thermal conversion process (see the calculation method for the latter in the supporting information). It is clear that the CO_2 conversion in our GA proceeds more energy efficient than pure thermal conversion. This is because the energy in the thermal conversion is distributed over all degrees of freedom based on the equipartition principle of energy, and thus it is especially spent on gas heating rather than on CO_2 dissociation reactions. In contrast, our GA clearly operates in non-equilibrium conditions, as the electrons have a much higher temperature than the gas itself (see our calculation results in section 4.3 below). These highly energetic electrons induce different chemical reactions, which normally do not occur at the considered gas temperate in case of equilibrium conditions.

In spite of the reasonable results obtained already by the gliding arc, the conversion should still be further improved, while maintaining the high energy efficiency. More specifically, if this low conversion could not be further improved, it would imply the need for operating in a recycle mode, which would make the system highly non-effective.

4.3 Typical GA discharge characteristics

In order to understand the time behavior of the plasma characteristics in the CO_2 GA, we plot in figure 4 the electron number density, electron temperature, gas temperature, as well as of the CO molar fraction distribution, at different moments in time, for a gas flow rate of 2.5 L/min and a discharge power of 40 W.
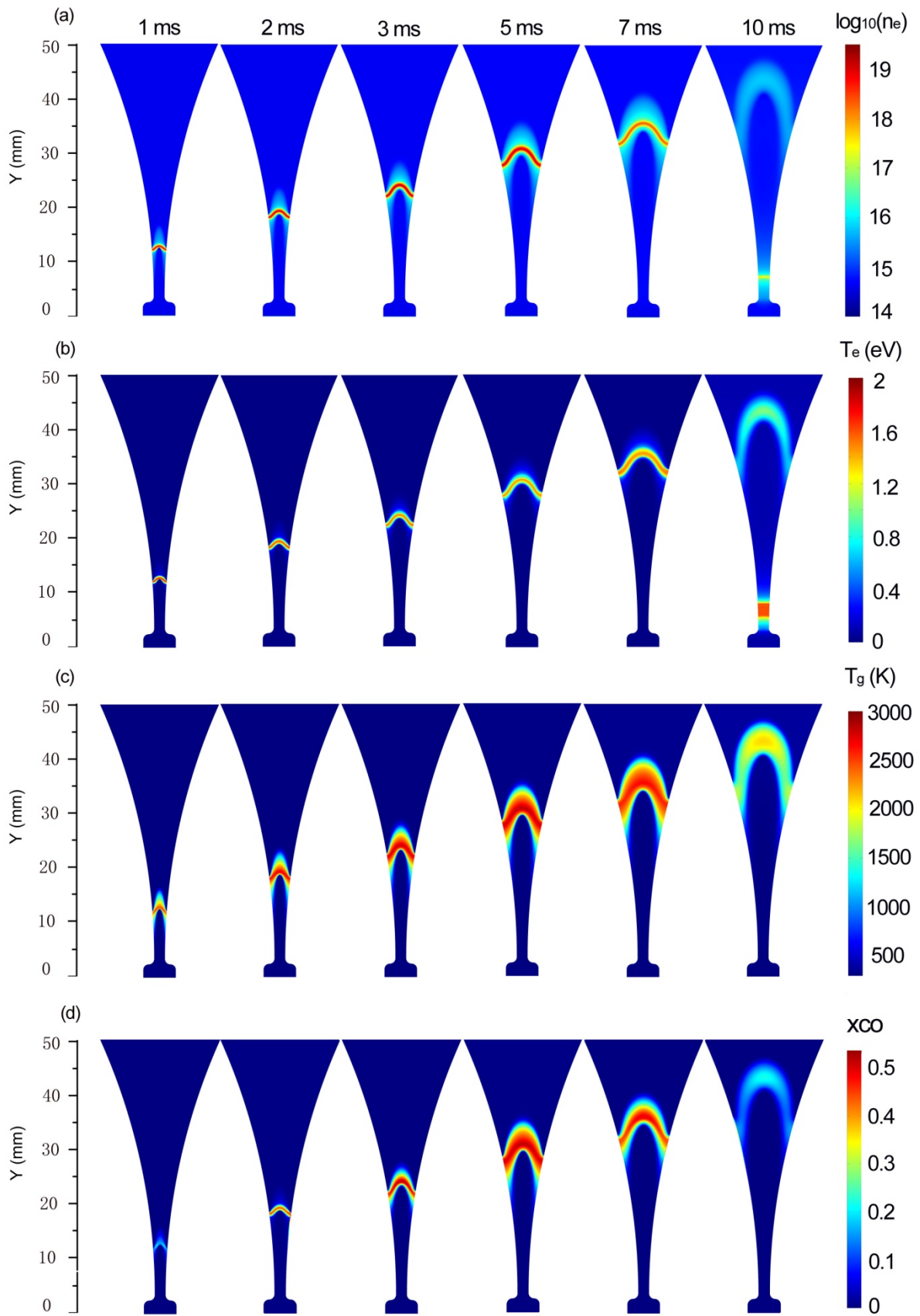
Figure 4 Time evolution of the electron number density (in m^{-3}), electron temperature, gas temperature and CO molar fraction distribution, at a gas flow rate of 2.5 L/min and a discharge power of 40 W.

The results are plotted starting from t = 1 ms. At *t* = 0 ms, the source voltage is larger than the critical breakdown voltage with a shortest gap separation of 2 mm. The discharge ignition takes place, because of a positive value of the net electron generation, yielding an abrupt increase of the electron number density during the electrical breakdown. Once the conducting channel is established, the arc travels along the electrodes as a result of the gas flow drag. Since the gas velocity has a maximum value at the discharge axis and gradually decreases to zero at the electrode surface, the arc root moves at a much slower velocity compared to the arc body. Thus, the arc gradually begins to bend due to the gas blast. The maximum electron number density also increases due to the rising voltage and hence discharge current (see figure S1 in the supporting information), till a peak value is reached at 3.5 ms (see figure 4(a)). At later times, the discharge current drop, and consequently, the electron density follows the same trend till zero at t = 8.5 ms, when the applied voltage reaches zero (see figure S1). The GA gradually extinguishes and enters a relaxation stage, where the voltage is small and not enough to sustain the GA discharge. Thus, there is a decaying residual low density plasma moving downstream with the gas flow (see figure 4(a)). Shortly after t = 8.5 ms, the applied voltage of the alternating current (AC) power source changes its polarity (see figure S1 of the supporting information) and reaches again the critical breakdown voltage at the narrowest electrode gap separation of 2 mm, where a restrike occurs by establishing a new conducting channel. It should be noted that the re-ignition of the GA does not exactly take place at the shortest gap separation (Y = 2.5 mm), but at Y = 7.5 mm. This is because the local electric field at Y = 7.5 mm first reaches the critical breakdown field. This is in good agreement with our experiments, recorded by the digital camera (see figure S2 of the supporting information).

The rise and drop in electron number density during one GA discharge cycle results in an enhanced and reduced Joule heating effect before and after t = 3.5 ms, respectively. The Joule heating refers to the process by which the passage of an electric current through a conductive medium produces heat and causes heating of the electrons. Correspondingly, the electron temperature first increases and then decreases (see figure 4(b)). After t = 8.5 ms, the electron temperature of the residual GA channel continuously decreases, because the electron number density and the electric energy stored in the channel decay very rapidly. Subsequently, the extremely large reverse polarity voltage imposed across the electrodes at the shortest electrode gap leads again to an increase of the electron temperature and hence a subsequent breakdown at the new position of Y = 7.5 mm (see figure 4(b)).

Once the discharge is ignited, the electrons cause vibrational excitation of CO_2, and the energy stored in the vibrationally excited states will partially be transferred to the gas by vibrational-translational (V-T) relaxation. Indeed, at atmospheric pressure, the typical characteristic time for V-T relaxation in CO_2 is very short (around 10^{-5} s). As a result, the gas temperature also rises as a function of time, reaching a maximum value of about 2700 K at around t = 3.5 ms, when the applied source voltage (V_{source} = 7200sin($2\pi50t$ + 0.50)) and the discharge current reach their maximum (see figure 4(c)). Subsequently, the gas temperature in the arc channel gradually decreases to around 2000 K when a new cycle starts at t = 10 ms, because the discharge power decays rapidly in the relaxation stage from 8.5 ms to 10 ms.

The CO molar fraction is obviously equal to zero before the arc is formed, but it starts increasing gradually as a function of time, when the voltage and hence the discharge current in the arc rise, up to a value of 0.55 at *t* = 3.5 ms, indicating that CO_2 is gradually converted into CO. At later times, the

1   discharge current and hence the discharge power start to drop, so the CO molar fraction within the

2   arc channel gradually decreases until the arc is extinguished. This is caused by recombination of CO

3   and O into CO_2. Furthermore, new CO_2 gas will continuously be transported into the arc channel by

4   both diffusion and convection, while the dissociation products will leave the discharge channel by the

5   same transport mechanisms. This leads to a reduction of the maximum local CO molar fraction, as is

6   clearly indicated in figure 4 (d). Note that the overall CO_2 conversion is much lower than the local

7   conversion of 80%, which corresponds to the maximum CO molar fraction of 0.55 (and CO_2 molar

8   fraction of 0.2; see below). This is because the overall CO_2 conversion is calculated for the entire gas

9   passing through the reactor, integrated over the time of one GA cycle (i.e., 10 ms), and thus not only

10   for the fraction of gas passing through the active arc channel at a certain moment in time.
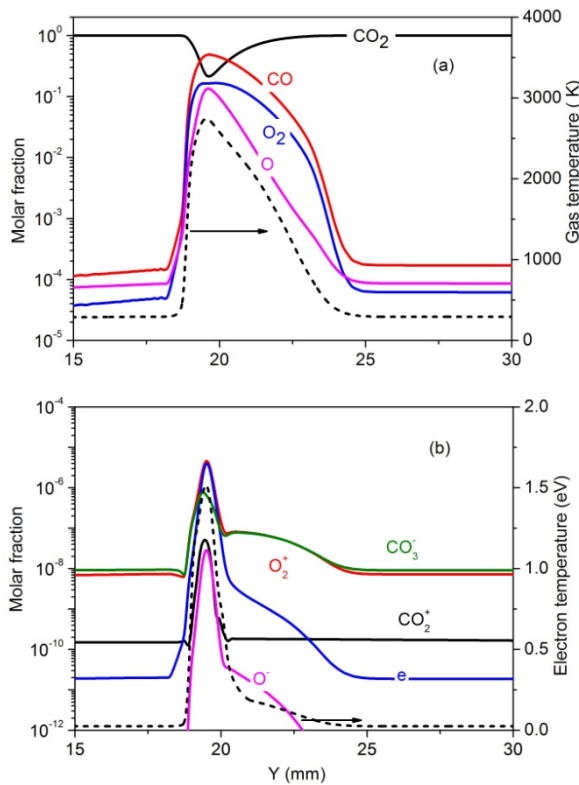
11
12 **Figure 5** 1D distribution of the molar fractions of the neutral species (a) and the charged species (b)

13   as a function of axial distance on the symmetry plane, at a time instant of 2.5 ms. The gas

14   temperature and electron temperature are also plotted in dashed lines in (a) and (b), respectively.

15   The molar fractions of the major neutral and charged species occurring in the CO_2 GA are plotted

16   as a function of Y position in figure 5, at a time instant of 2.5 ms, and at the same conditions as in

17   figure 4. It is clear that CO_2 is the major component in the plasma, except at the centre of the arc,

18   where the molar fraction of CO_2 (around 0.2) is lower than the fraction of CO (around 0.5), and

19   comparable to the molar fractions of O_2 (0.16) and O (0.14). This indicates that the majority of CO_2 is

20   split here into CO and O_2 as well as O atoms. Moreover, part of the O atoms have recombined into O_2

21   molecules, indicating a higher decay rate of the O molar fraction than that of O_2. The molar fractions

22   of CO, O and O_2 drop quickly when moving towards the outer part of the arc, indicating that most of

23   the CO_2 splitting takes place in the centre of the arc.

24   The CO_2 conversion can be further enhanced when applying a higher power, however, even at

25   100 W, the local molar fraction of CO_2 drops to extremely low values and the local conversion in the

GA reaches almost 100 %. This limits the further improvement of GA based CO_2 conversion. Therefore, the conversion can only be further enhanced if we can provide more CO_2 into the arc centre, while at the same time remove the dissociation products (CO and O_2) out of the arc centre. This will be further discussed in detail in section 4.5.

The molar fractions of the various charged species are at maximum 10^{-5}, even in the arc centre, and they clearly drop upon larger distance from the centre of the arc. Also the electron molar fraction is at maximum 10^{-5}, indicating that the CO_2 plasma is only weakly ionized, even in the centre of the arc. The major positive ions are the O_2^+ ions, while the CO_3^- ions are the major negative ions, and they are even more important (although still with very low molar fractions) than the electrons, except in the centre of the arc. These trends are in agreement with our previous findings obtained by a 1D cylindrical discharge model, despite the considerable number of approximations adopted there [41].

The gas temperature and electron temperature are also plotted in figure 5. They both reach their maximum in the centre of the arc, as is logical, and they drop significantly as a function of position from the arc centre. The electron temperature reaches a maximum of 1.5 eV (or 17,400 K) in the centre of the arc at the time instant of 2.5 ms, but it drops significantly as a function of rising distance from the arc centre in the first 0.5 mm, followed by a slower decay to thermal values at a distance of about 1.0 mm from the centre. The gas temperature is at maximum about 2700 K in the centre of the arc. From the comparison between these temperatures, it is clear that the gliding arc is far from thermal equilibrium, as the electron temperature is about 6 times higher than the gas temperature. As mentioned in section 4.1 above, a gas temperature up to around 2700 K and an electron temperature up to 1.5 eV correspond well to experimental data found in literature for low current atmospheric pressure GA discharges, although it should be mentioned that it is not easy to compare different GA setups with different reactor geometries and discharge conditions.

4.4 CO_2 conversion mechanisms in the GA

In order to evaluate which mechanisms are the most important for the CO_2 splitting in the GA plasma, and how they can eventually be further improved, we investigated the dominant reaction pathways for the formation and loss of CO_2 for the same conditions as in figure 4. The reactions are listed in table 3 and their relative contributions to the overall CO_2 loss and formation are presented in figure 6. This kinetic analysis was performed by looking at the time and volume integrated rates of the various processes for a complete gliding cycle of 10 ms. In the supporting information, we also plot the temporal evolution of the most important loss and formation rates of CO_2, obtained by integrating the reaction rates over the entire reactor (see figure S4).

Table 3 Dominant CO_2 loss and formation reactions.

Process	Loss reaction	Process	Formation reaction
L1v	$e + CO_2(v) \rightarrow e + CO + O$	F1	$CO + O_2 \rightarrow CO_2 + O$ [a]
L1g	$e + CO_2(g) \rightarrow e + CO + O$		
L2v	$CO_2(v) + O \rightarrow CO + O_2$	F2	$CO + O + M \rightarrow CO_2 + M$
L2g	$CO_2(g) + O \rightarrow CO + O_2$		
L3v	$CO_2(v) + M \rightarrow CO + O + M$	F3	$CO + O^- \rightarrow e + CO_2$
L3g	$CO_2(g) + M \rightarrow CO + O + M$		
L4v	$CO_2(v) + O^- + M \rightarrow CO_3^- + M$		
L4g	$CO_2(g) + O^- + M \rightarrow CO_3^- + M$		

(a) O_2 represents the sum of the ground state and the vibrational states of molecular oxygen.
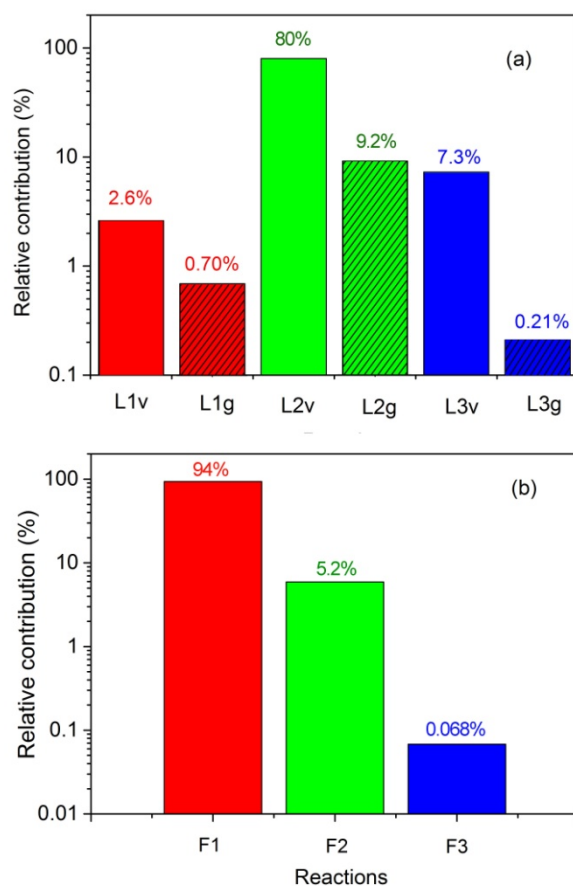
Figure 6 Relative contributions of the most important processes for CO_2 loss (a) and formation (b). The reaction numbers in the x-axis correspond to the numbers in table 3. Note that only the three main loss processes are illustrated, as the fourth process (L4v, L4g) contributes for less than 0.1 %.

The most important process for CO_2 loss is the dissociation of vibrationally excited states of CO_2 upon collision with O atoms (L2v) with a relative contribution of about 80 %. The same process, but upon collision of ground state CO_2 with O atoms (L2g) has a relative contribution of 9.2 %. Furthermore, the dissociation of vibrationally excited states of CO_2 upon collision with any neutral species (M) also contributes for 7.3 % (L3v). The relative contribution of the same process, but starting from ground state CO_2, is only 0.21 % (L3g). Besides, electron impact dissociation from the CO_2 vibrational levels (L1v) and from the CO_2 ground state (L1g) contribute for 2.6 % and 0.70 %, respectively. Compared with the electron impact dissociation reactions, the neutral reactions upon collision with O atoms have a lower energy requirement [19] and hence are more energy efficient. Note that reactions L2v and L2g are actually follow-up reactions of reactions L1v and L1g, as the O atom that reacts in reactions L2v and L2g is the result of CO_2 splitting, either by reactions L1v and L1g, or reactions L3v and L3g. Nevertheless, once the first O atoms are formed upon CO_2 splitting, the reactions L2v and L2g can occur in parallel to these other reactions, and thus we can consider them separately in this analysis.

Our calculation results reveal that the CO_2 dissociation mainly proceeds from the vibrationally excited levels of CO_2. The latter provide more energy efficient dissociation, because the vibrational energy can help overcome the activation energy barrier of the reaction and thus increase the reaction rate constant [26]-[27]. This is consistent with experimental investigations in literature. Indeed, experimental work for both a diverging electrodes gliding arc reactor [5] and a gliding arc

16

plasmatron [6] shows that the presence of a very small quantity of water added into CO_2 greatly reduces the power efficiency compared with pure CO_2 at atmospheric pressure. This is explained by the fact that water can significantly reduce the vibrational excitation of CO_2 molecules, because the energy is absorbed and quickly lost by water. Based on this, Nunnally et al. [6] concluded that non-equilibrium vibrational excitation plays the major role during CO_2 dissociation in a gliding arc.

Additionally, there exist measurements in the literature, demonstrating that the vibrational temperature in the gliding arc is higher than the gas temperature, even at atmospheric pressure, although we cannot validate our model by direct comparison, as experimental data for the vibrational temperature in pure CO_2 in classical gliding arc reactors do not yet exist. However, in a non-equilibrium gliding arc "tornado" discharge using CO_2 doped with 1% N_2 at a flow rate of 10 lpm and a power of 200 W, Nunnally et al. [49] estimated the vibrational temperature to be approximately 6000 K at atmospheric pressure, by comparing the theoretical and experimentally measured spectra for the N_2 system, and this value is much higher than the reported rotational gas temperature of 2700K ± 50K. Therefore, these experimental results support our modelling results.

Some of the reactions plotted in figure 6(a) also occur in the opposite direction, hence, besides dissociation of CO_2, the recombination of CO with O_2, O and O^- ions also takes place in the GA, giving rise to the formation of CO_2 again and yielding a lower net conversion of CO_2. The recombination reaction of CO with O_2 molecules (F1, i.e., the opposite of L2) is the predominant production process of CO_2, with a relative contribution to the overall CO_2 formation amounting to 94 %. The recombination reaction of CO with O atoms (F2, i.e., the opposite of L3) has a relative contribution of 5.2 %, while the recombination of CO with O^- ions (F3) only contributes for 0.068 %. Other reactions play a negligible role towards CO_2 formation (< 0.05 %).

Note that the reverse reactions, especially the recombination of CO with O_2 molecules, have only slightly lower rates than the rates of the most important loss processes, as depicted in figure S4 in the supporting information. Therefore, these reactions have a detrimental effect on the overall CO_2 conversion. Indeed, when the rates of these reactions would become even larger, they would inhibit further CO_2 dissociation. This happens when a considerable fraction of the CO_2 molecules is already converted into CO and O/O_2, and especially at high gas temperature in the arc. When comparing the total loss of CO_2, integrated over the entire arc and the whole gliding cycle, with the total formation of CO_2, we obtain values of 3.8 x 10^{18} vs 3.5 x 10^{18} at the conditions under study. Thus, it is clear that about 92 % of the CO_2 converted in the GA, will be formed again, so the net conversion of CO_2 into CO is much smaller than the initial loss of CO_2. Therefore, the recombination of CO with O_2 back into CO_2 is clearly a limiting factor, which affects the further improvement of GA based CO_2 conversion and its energy efficiency. This will be discussed in the next section.

4.5 How to improve the CO_2 conversion and energy efficiency in the GA ?

From previous section, we can clearly identify the limiting factors for energy efficient CO_2 conversion in the GA. Therefore, in this section, we will propose solutions on how to further improve the performance of the GA for energy efficient CO_2 conversion. First we will discuss the role of the vibrational levels in energy efficient CO_2 conversion. Subsequently, we will look in more detail at the recombination of CO with O_2, which contributes mostly to the CO_2 formation at the conditions under study. Finally, we will elaborate on some ways to increasing the velocity difference between the GA and the gas flow, which can increase the fraction of CO_2 that can be processed by the arc, and hence improve the conversion.
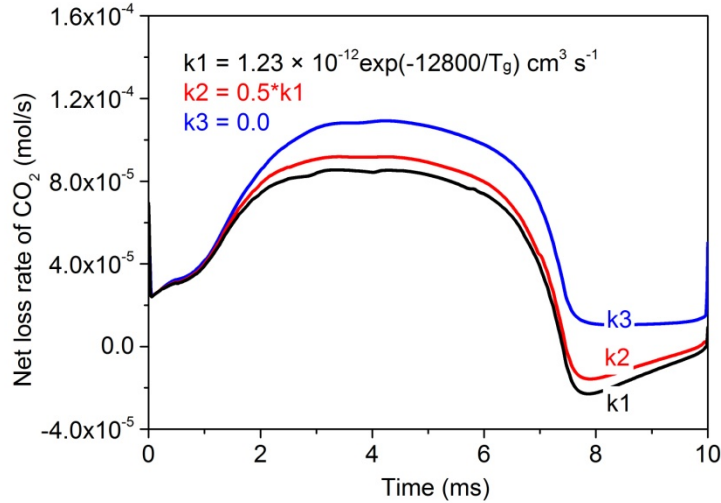
4.5.1 Promoting the vibrational kinetics

It is clear that non-equilibrium vibrational excitation of CO_2 promotes energy efficient dissociation in the GA. This is also consistent with experimental investigations in literature [6]. Our results indicate that the population of the symmetric mode levels and the lower asymmetric stretch mode levels is much higher than that of the higher asymmetric mode levels. Therefore, these lower vibrationally excited levels mostly account for the total CO_2 conversion, although there is still some overpopulation for the higher levels. The reason why especially the lower vibrational levels contribute to the CO_2 conversion is because the vibrational energy distribution function tends to become more thermalized at high gas temperature [73]. Indeed, the energy exchange upon collision between vibrational levels and ground state molecules, which depopulates the vibrational levels, i.e., so-called VT relaxation, increases with gas temperature. Therefore, we should look for ways of inhibiting the VT relaxation process to increase the degree of overpopulation of the higher asymmetric mode levels.

A recent kinetic modelling of microwave plasma based CO_2 conversion has shown that lower pressures, lower gas temperature and higher power densities (at least for pressures below 300 mbar) lead to more vibrational excitation, which is beneficial for the conversion [73]. However, our GA operates at atmospheric pressure, which is more convenient for industrial applications, so the solutions of reducing the gas pressure and increasing the power density (which only has beneficial effect at a pressure below 300 mbar [73]) are not practical. Therefore, we believe that the gas temperature should be reduced, to inhibit the VT relaxation, and thus to promote the role of the higher vibrational levels, and hence the conversion and energy efficiency. In this respect, enhancing the mixing between the GA and the cold gas can help to realize this goal, which was clearly indicated by our previous modelling for a 1D gliding arc [41] and by experimental work [6]. Furthermore, reducing the gas temperature will also result in a lowering of the recombination reactions, thus also improving the overall CO_2 conversion (see next section). On the other hand, it will also lead to a drop in the dissociation rate constants by neutral particle collisions, and this has a detrimental effect on the conversion. Therefore, an optimized gas temperature should exist for GA based CO_2 conversion, where the beneficial effect of a lower temperature, due to (i) a more pronounced non-equilibrium population of the highly excited vibrational levels, and (ii) lower recombination rates of CO back into CO_2, exceeds the detrimental effect by the lower dissociation rate constants of dissociation upon collision with neutral particles. Finding out this optimal temperature is, however, not so straightforward with our 2D model, as the latter self-consistently calculates the gas temperature and it is not an input in the model. For this purpose, a 0D model, where the gas temperature can be introduced as an input parameter, could be more suitable [40].

Besides, because electron impact vibrational excitation of CO_2 is mainly important for reduced electric field values (i.e., ratio of electric field over gas density) below 80 Td [72] (where 1 Td = 10^{-21} V/m^2), we should target to actively tune the reduced electric field to these values, by optimizing the reactor electrical operating parameters. Finally, increasing the electron number density will also promote the vibrational excitation and thus selectively deliver energy to this most energy efficient CO_2 dissociation pathway. It has been reported in literature [66] that adding noble gases, such as argon, to CO_2 would improve the CO_2 conversion and energy efficiency by increasing the electron number density, because argon has a lower breakdown voltage than CO_2.
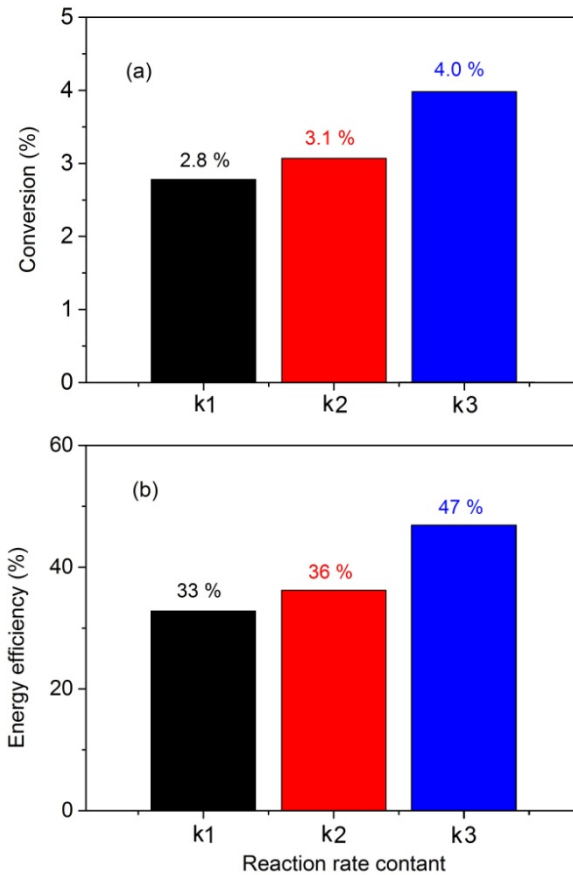
4.5.2 Reducing the recombination of CO with O_2

Figure 7 Effect of different rate coefficients of the recombination reaction ($CO + O_2 \rightarrow CO_2 + O$) on the calculated net loss rate of CO_2, integrated over the entire reactor volume, at the same conditions as in figure 4.

It is clear from section 4.4 that the recombination reaction (F1), i.e., $CO + O_2 \rightarrow CO_2 + O$, is mainly limiting the CO_2 conversion and energy efficiency. In our model, we adopted the rate coefficient as proposed by Fridman [19]. However, to evaluate the effect of this recombination reaction on the overall CO_2 conversion, we have performed some further simulations in which (i) we reduced the rate coefficient of this reaction by 50%, and (ii) we completely removed this recombination reaction from the model, as indicated in the legend of figure 7.

It is obvious from figure 7 that a lower rate coefficient of the recombination reaction yields a higher net CO_2 loss rate. The CO concentration within the GA channel, and hence the influence of the recombination reaction on the CO_2 formation, is minor till t= 1.7 ms. As a result, the different rate coefficients have a negligible effect on the net loss rate of CO_2 up to 1.7 ms. Upon increasing CO concentration, the different rate coefficients do cause some deviation in the calculated net loss rates of CO_2. After t = 7.5 ms, the formation rate of CO_2 is even larger than the loss rate for k1 and k2, leading to a negative value of the net CO_2 splitting rate. Of course, integrated over the entire GA cycle, the overall CO_2 loss (or conversion) rate is still positive, but it is greatly reduced due to this important backward (recombination) reaction.

Figure 8 Effect of using different rate coefficients of the recombination reaction (CO + O_2 → CO_2 + O) on the calculated CO_2 conversion (a) and energy efficiency (b), for the same conditions as in figure 7. See legend of figure 7 for the values of k1, k2 and k3.

Figure 8 shows the conversion and energy efficiency, calculated with the original rate coefficient (k1) [19], in comparison with the results obtained when this rate coefficient is divided by 2 (k2), as well as when the recombination reaction is removed from the model (k3). The conversion and energy efficiency increase only slightly when the recombination rate coefficient is divided by 2, while they rise from 2.8 % to 4.0 %, and from 33 % to 47 %, respectively, by removing the recombination reaction (CO + O_2 → CO_2 + O) from the model. Although the conversion is still low, the energy efficiency rises significantly. This clearly indicates that reducing the recombination of CO with O_2 is quite promising to enhance the CO_2 conversion and (especially) the energy efficiency.

To achieve this objective, we suggest to apply possible scavengers, catalysts or separation membranes, in order to remove the O_2 molecules [31]. These are only suggestions, and they should of course be experimentally explored to evaluate the possibilities. On the other hand, the combination of a solid oxide electrolyser cell with a plasma set-up was already illustrated in [74] to be beneficial for the CO_2 conversion, and it works according to the same principle. In this way, the local concentration of O_2 molecules within the arc channel, and hence the net formation of CO_2 by the recombination reaction (CO + O_2 → CO_2 + O), could be reduced, because there is not enough reactant (O_2) available for the backward reaction from CO into CO_2 (F1).

H$_2$ or CH$_4$ could act as possible scavengers for atomic oxygen, forming H_2O. This possibility was already illustrated to be beneficial for O trapping in literature, based on a combined plasma chemical

kinetics model and experiments for CO_2 conversion in another type of plasma [75]. The trapping of O atoms might be able to promote the CO_2 conversion by (i) inhibiting the recombination reaction F2 [40], and (ii) by avoiding the formation of O_2, which will inhibit the recombination reaction F1. Experiments in literature have indeed revealed that the addition of H_2 or CH_4 in a GA reactor can improve the conversion of CO_2 [6],[54], but the enhanced conversion of CO_2 cannot be simply, or entirely, attributed to the inhibited recombination reactions. This is because the H atoms or CH_x radicals produced by H_2 or CH_4 dissociation can also contribute to CO_2 dissociation. Moreover, the removal of O atoms will also inhibit the dominant mechanism of CO_2 splitting, i.e. the dissociation of CO_2 upon collision with O atoms (L2v, L2g) and thus it might also exhibit a negative effect on further improving the CO_2 conversion. Therefore, the reason why adding H_2 or CH_4 promotes the CO_2 conversion is not necessarily attributed to their scavenging role in consuming the O atoms. Indeed, the direct involvement in CO_2 splitting by the reversed water gas shift reaction ($CO_2 + H_2 \rightarrow CO + H_2O$) has been verified to be a very important path for CO_2 splitting into CO when CH_4 [54] or H_2 [6] is added into a CO_2 GA plasma. Moreover, the addition of H_2 or CH_4 can increase the electron density by inhibiting electron attachment to O_2 (which is an electronegative gas), and this can also contribute to a higher CO_2 conversion.

The idea of using a catalyst with a high surface interaction for O atoms to recombine into O_2 [76] or for O_2 adsorption is probably not very effective, because the O_2 molecules would be released back to the plasma phase and again undergo recombination with CO. In contrast, a more advanced catalytic process would be an alternative form of chemical looping, in which the O or O_2 is captured in the plasma set-up and then used as oxidizing agent in a second set-up [77]-[78]. However, this is only a concept, and has not be demonstrated yet for a GA reactor.

The third method, based on separation membrane technology, would transport the O_2 molecules (or O atoms) away from the reaction mixture. For example, by combination of a solid oxide electrolyser cell with a plasma set-up, Tagawa et al. [74] and Mori et al. [79]-[80] have observed an increasing CO_2 conversion by placing an O_2 trapping membrane into a CO_2/CH_4 or CO_2 discharge, in order to separate O_2 from the reaction mixture.

Besides the effect of possible scavengers, catalysts or membranes to remove the oxygen, as mentioned above, we believe that the recombination of CO with O_2 could also be avoided or minimized by providing effective quenching of the high temperature in the arc zone, due to mixing with cold gas at very fast cooling rates. This could be especially beneficial in the relaxation stage of the GA (around 8 ms) when the discharge current is low, and the CO_2 loss rate is minor, but the recombination rate of CO with O_2 is still very large due to the very high gas temperature, leading to net CO_2 formation. Indeed, an effective quenching of the residual plasma temperature can help to decrease the recombination reaction rate and inhibit the CO_2 formation in this stage, leading to an improved conversion and energy efficiency. We believe that such a quenching of the plasma temperature could be realized by improving the reactor geometry and/or optimizing the flow conditions, but further studies are needed to elaborate on these solutions.

4.5.3 Increasing the CO_2 fraction to be treated by the arc due to a velocity difference between GA and gas flow

Besides promoting the vibrational kinetics and reducing the recombination reaction of CO into CO_2, another way to improve the CO_2 conversion would be to enhance the CO_2 fraction to be treated

1   by the arc, by better mixing of the GA and the cold gas flow. This can be realized when there is a
2   velocity difference between the GA and the gas flow. Several experimental studies indeed have
3   shown that the arc gliding velocity can be slightly lower than the gas velocity [14], [33]. We present
4   here some simulation results, showing that there can indeed be a (small) difference between the arc
5   and gas flow velocity. We can distinguish two different ways to realize this.

6   **(1) Smooth velocity difference due to the arc bending**
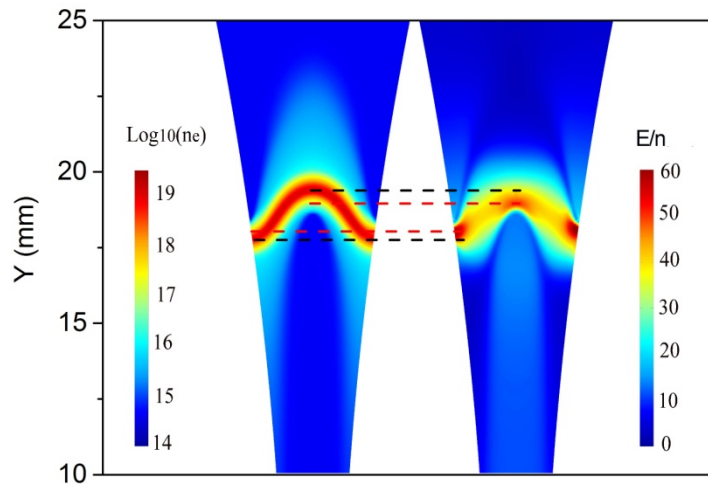
7
8   **Figure 9** 2D distribution of the electron number density (left, in m^{-3}) and reduced electric field (right,
9   in Td) at a time instant of 2.5 ms for the same conditions as in figure 4. The black and red lines
10   indicate the position of the arc center and of the maximum reduced electric field, respectively,
11   showing that they are separated, leading to extra ionization downstream the arc in the centre, and
12   consequently to slowing down of the arc movement.

13   The first possible reason for a lower arc velocity vs gas flow velocity is related to the arc bending,
14   and thus the existence of zones with increased electric field outside the arc centre. The latter indeed
15   leads to a separation of the arc centre (with the maximum electron number density) and the position
16   with maximum reduced electric field, as presented in figure 9. This is caused by the fact that in the
17   symmetry plane, when the arc is highly bended, some parts of the arc in the downstream region of
18   the arc centre are positioned closer to each other. This increases the electric field strength in this
19   region and causes a gradual ionization of the gas in the downstream region. The latter will result in a
20   slightly lower arc velocity compared to the gas velocity. Likewise, near the walls (cathode and anode),
21   the maximum reduced electric field, and hence the gradual ionisation, appears in the upstream
22   region of the arc centre, which results in a slightly higher arc velocity than the gas velocity. Thus, the
23   GA moves a bit slower than the gas flow in the central part of the reactor and a bit faster in the
24   regions near the walls. At t = 2.5 ms, our calculation predict a GA velocity of 5.9 m/s in the centre,
25   compared to a gas flow velocity of 7.4 m/s. The ratio of gas velocity to arc velocity is thus 1.2, which
26   is in reasonable agreement with experiments [14], [33].

27   We have also performed calculations at higher gas flow velocity, and the results show that this
28   leads to an increased velocity difference between the arc and gas flow. For example, with the same
29   gas flow rate of 2.5 L/min, assuming the flow passing through a channel with depth of 1 mm, which is
30   only half of the value in our standard model, the gas flow velocity at the same time instant t = 2.5 ms
31   was calculated to be 8.3 m/s, with a GA velocity of 5.8 m/s, thus yielding a ratio of gas velocity vs arc

velocity of 1.4. This clearly shows that the velocity difference between GA and gas flow will be higher for higher gas flow velocities, which is also reported in experiments [14], [33]. Correspondingly, our calculated conversion increases from 2.78 % to 4.4 %, although the energy efficiency only increases from 32.8 % to 34 %. Although this is an artificial method, we can show in this way that the treatment capacity can be enlarged by increasing the local gas velocity and hence the relative velocity between gas flow and GA. Increasing the local gas velocity can be realized by modifying the reactor setup and hence the flow configuration at a fixed gas flow rate, for example by shortening the narrowest gap separation of both electrodes [40] or by reducing the distance between the nozzle exit and the reactor [81] or by decreasing the nozzle internal diameter [82]. Indeed, following such methods, increased conversions were reached experimentally [40], [81] and [82]. However, we should also mention that simply adjusting these parameters is not a proper way to enhance the treatment capacity of the GA reactor, because it might give rise to an extreme increase in the gas velocity, which may greatly reduce the effective residence time of CO_2 in the GA volume. This is of course detrimental for the CO_2 conversion. Moreover, the high gas velocity will bring a strong cooling effect and hence a lower gas temperature; the latter can be beneficial (to promote the vibrational kinetics and/or reduce the recombination reactions), but it may also be detrimental (due to the reduced dissociation reaction rate constant), as we discussed in section 4.5.1 above. Therefore, the above mentioned operating parameters should be optimized in a suitable range, to guarantee an improvement in conversion and energy efficiency [83].

(2) Sudden velocity difference due to back-breakdown events

Besides the smooth reduction in GA velocity explained above, another reason for the lower arc velocity vs gas flow velocity is related to the instabilities of the arc and to secondary breakdowns, also called back-breakdown, causing a reduction in arc length [84].

The back-breakdown phenomena, which result in a fast shortening of the arc as a result of breakdown between different parts of the arc (instead of between the electrodes) often take place in a GA, especially at higher gas flow rates, as also mentioned in section 4.1. These shortcuts effectively appear as a lag of the arc velocity compared to the gas flow and could be an efficient mechanism for the treatment of a larger gas fraction. As explained at the end of section 4.1, this effect is not taken into account in previous sections, because at the gas flow rate of 2.5 L/min, our high speed camera did not record any back-breakdown events.
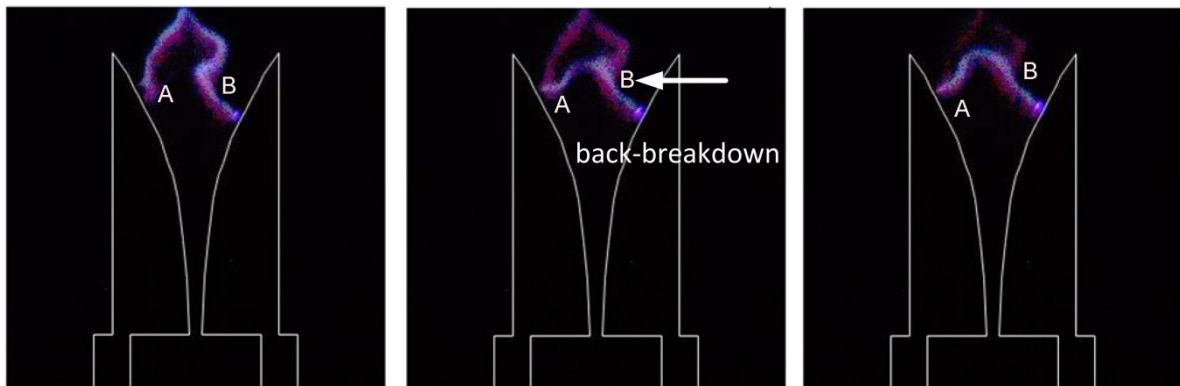
Figure 10 Back-breakdown event recorded by the high speed camera at a flow rate of 5 L/min (5000 frames/s, exposure time of 50 μs, electrode throat of 2.0 mm)

1   Figure 10 illustrates a back-breakdown event, recorded by the high speed camera at a flow rate

2   of 5 L/min. Indeed, at a high gas flow rate (above 2.5 L/min), the GA discharge is unstable and it has a

3   rather irregular shape. When some parts of the GA (see points A and B in figure 10) get closer to each

4   other, the electric field there increases. Once the potential difference between these two parts, and

5   hence the local electric field, exceeds the critical breakdown electric field [85], a new discharge

6   channel is established (see middle panel) and the old discharge channel disappears very fast. This

7   causes a drop in the GA velocity as compared to the gas flow velocity.

8   Although several experiments [36],[84] have been performed to study the back-breakdown

9   events, it is not straightforward to establish a self-consistent back-breakdown model, since this

10   behaviour is mostly stochastic by nature and the arc instabilities are not well defined. To investigate

11   here the influence of the back-breakdown events on the CO_2 conversion, we have initiated this

12   process by establishing an artificial plasma channel, which is triggered on a regular or irregular basis

13   with respect to the arc path or time, i.e., after every certain distance or period. Details on how the

14   back-breakdown model is established can be found in [38], as well as in the supporting information

15   of our paper.

16

17
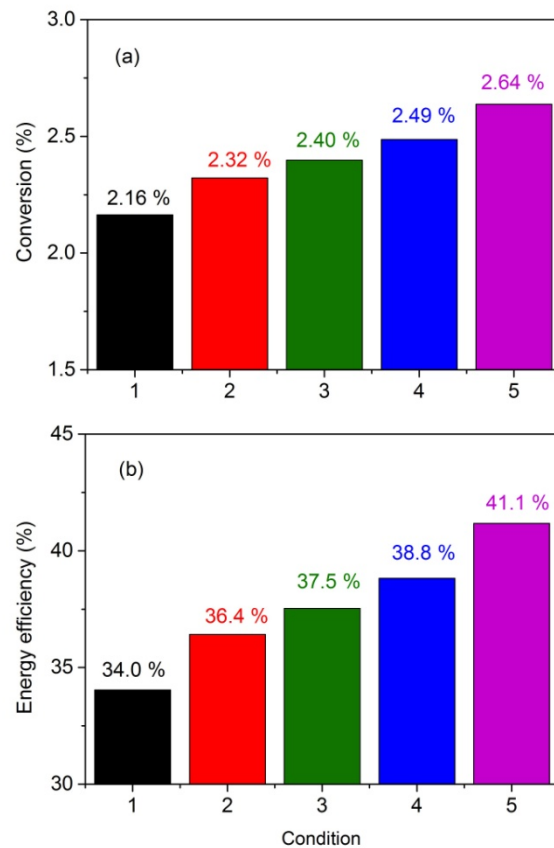
18   **Figure 11** Effect of the back-breakdown events on the CO_2 conversion and energy efficiency at a gas

19   flow rate of 5.0 L/min, for different cases, i.e., without back breakdown (1); one back-breakdown at 5

20   ms (2); a two back-breakdowns, at 5 ms and 6 ms (3); three back-breakdowns, at 5 ms, 6 ms and 7 ms

21   (4); and five back-breakdowns, at 5 ms, 5.5 ms, 6 ms, 6.5 ms and 7 ms (5).

22   Figure 11 illustrates the effect of the back-breakdown events on the calculated conversion and

23   energy efficiency. The power needed to initiate the back-breakdown events is included in the

24   determination of the total plasma power and hence in the SEI value in Eq. (3), as well as the

calculation of the energy efficiency in Eq. (4) (see section 2). It is clear that the back-breakdown events yield an improved CO_2 conversion and energy efficiency, compared with the case without back-breakdown, because a larger fraction of CO_2 is treated by the newly established discharge channel. This also explains why a larger number of back-breakdown events can enhance the CO_2 conversion and energy efficiency (see cases 2, 3, 4 and 5). Moreover, more back-breakdown events also result in a lower overall gas temperature, as is clear from figure S7 of the supporting information, because the heat is now spread over a larger domain and not only within the initial arc channel. This lower gas temperature can have beneficial or detrimental effects on the overall CO_2 conversion, as explained above.

As discussed above, the occurrence of the back-breakdown events is closely linked with two factors, i.e. the arc instabilities and a sufficiently high arc voltage drop. The former leads to a rather irregular arc shape and a non-stable discharge, increasing the probability of a closer interaction between two separated parts of the GA. The latter can ensure a high enough electric field between the two separated parts of the arc, to ignite a new discharge channel. In order to satisfy these two essential requirements, besides increasing the gas flow rate, the gas flow velocity must also be increased by modifying the reactor setup and hence the flow configuration under a fixed gas flow rate, as discussed above.

4.5.4 Summary of the proposed improvements
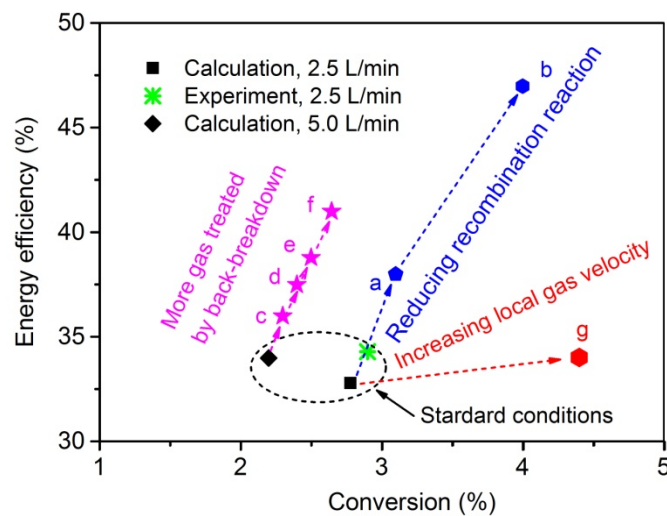
Figure 12 Energy efficiency vs CO_2 conversion in our GA reactor, as obtained by our experiments and calculated by our model, for the standard conditions (indicated with the oval), as well as several improvements as predicted by the model, by either (i) reducing the recombination rate coefficient from k1 to k2 (a) and k3 (b) (cf. figure 7), or (ii) enhancing the treated CO_2 fraction, by increasing the number of back-breakdown events, from 1 (c) to 2 (d) to 3 (e) to 5 (f), applicable at a higher gas flow rate (5 L/min), or (iii) by increasing the local gas velocity at the same gas flow rate, due to reactor inlet modifications, leading to a higher velocity ratio between gas flow and GA (g).

Finally, in figure 12, we schematically summarize the improvement in the CO_2 conversion and energy efficiency, as proposed and predicted by our model. The CO_2 conversion and energy efficiency are about 2.78 % and 32.8 % (calculated) or 2.90 % and 34.3 % (measured) at the standard conditions investigated, i.e., a gas flow rate of 2.5 L/min and a plasma power of 40 W, corresponding to a SEI of 0.25 eV/molecule. However, these values can be improved according to the model predictions, up to

a conversion of nearly 4 % and a corresponding energy efficiency of 47 % (see point b) by inhibiting the recombination reaction of CO with O_2. Furthermore, if the gas fraction that can pass through the arc zone could be enhanced, for instance by modifying the reactor setup and hence the flow configuration to realize a higher relative velocity between arc and gas flow, the conversion and energy efficiency are predicted to increase to 4.4 % and 34 %, respectively (see point g). Finally, the occurrence of back-breakdown events, which induce an abrupt difference in gas flow velocity and GA velocity, in case of a gas flow rate of 5 L/min (where the back-breakdown events indeed can take place), can also help to increase the conversion, although the effect seems to be rather limited, with a maximum conversion up to 2.6 %, while the energy efficiency would increase up to 41 % (see point f).

The proposed solutions yield some improvement in conversion and energy efficiency, but these model predictions still need to be verified by experiments. We hope that our model predictions will inspire experimental researchers to try out these modifications. Furthermore, the improvements are probably still too limited for industrial application of the GA for CO_2 conversion. Indeed, although the energy efficiency is quite good, the conversion is still very limited. Hence, more drastic modifications would be needed, e.g., in the gas flow pattern or the source design, to significantly increase the fraction of gas that can pass through the arc. One possible suggestion would be the reverse vortex flow gliding arc, which is based on cylindrical electrodes, and which allows a larger fraction of the gas to pass through the arc, yielding higher CO_2 conversions, as demonstrated by [6], [50] and **Error! Reference source not found.**.

2 Conclusions

In this work we studied the CO_2 conversion in a GA plasma, by means of a combined experimental and 2D modelling approach. We compared our measured and calculated CO_2 conversion and corresponding energy efficiency, as well as the electron number density in the arc, and obtained reasonable agreement. This indicates that our model can provide a realistic picture of the plasma chemistry and can be used to elucidate the underlying mechanisms and the dominant reaction pathways for the GA based CO_2 conversion.

We presented the typical arc plasma characteristics, such as the electron number density, electron temperature and gas temperature, as well the CO molar fraction, for one entire arc gliding cycle, as calculated by our model. These results clearly show that the GA plasma has a strong non-equilibrium character, because the electron temperature is much higher than the gas temperature, and the highly energetic electrons can induce several different chemical reactions. This explains the better performance of the GA for CO_2 conversion, yielding a much higher energy efficiency for a fixed value of the conversion, than pure thermal conversion, for which the energy is distributed over all degrees of freedom, including those not effective for the CO_2 conversion.

We also performed a chemical kinetics analysis of the modelling results, which enables us to identify the important species and reactions playing a role in the CO_2 splitting, i.e., the main production and loss pathways of CO_2. This allows us to gain sufficient insight into the entire process, and to identify the limiting factors for CO_2 conversion, and thus to propose solutions for improving the CO_2 conversion. Our model predicts that the most important process for CO_2 conversion is the dissociation of vibrationally excited states of CO_2 upon collision with O atoms, indicating that the CO_2 vibrational levels significantly contribute to the CO_2 dissociation. This can explain the good energy efficiency of CO_2 conversion in a GA plasma, as compared to some other plasma types.

We believe that, when it is possible to actively tune the reduced electric field (i.e., E/n ratio) in the plasma, by optimizing the reactor electrical operating parameters, or when we can increase the electron number density, as well as inhibit the VT relaxation processes by decreasing the gas temperature, we should be able to further promote the vibrational excitation and selectively deliver energy to the CO_2 dissociation via this energy efficient pathway. This should lead to some further improvement in the energy efficiency of CO_2 conversion in the GA.

Furthermore, our calculation shows that the reverse reactions, especially the recombination of CO with O_2 molecules (and to a lower extent with O atoms), have a non-negligible rate, compared to the CO_2 loss rate. Therefore, these reactions have a detrimental effect on the overall CO2 conversion. Thus, in order to further improve the CO_2 conversion, the reversion reactions should be inhibited or at least reduced. We clearly demonstrate this by running the model with different reaction rate coefficients for recombination, and when this recombination reaction is entirely removed, the calculated CO_2 conversion and energy efficiency rise from 2.8 % and 33 %, to 4.0 % and 47 %, respectively.

Finally, our simulation shows that the molar fraction of CO_2 within the arc center is very low, indicating that the local CO_2 conversion is nearly complete, but because the fraction of treated CO_2 within the arc is very limited, the overall CO_2 conversion is also limited. Therefore, we should look for ways to increase the CO_2 fraction to be treated by the arc, in order to further improve the GA based CO_2 conversion. Increasing this treated gas fraction can be realized when there is a velocity difference between the GA and the gas flow, so that new fractions of the CO_2 gas can pass through the arc, while the converted fraction (i.e., CO, O and O_2) will leave the active arc region, before it can recombine back into CO_2. We therefore discuss possible ways of increasing the relative velocity between GA and gas flow. The first way to realize this is by increasing the local gas velocity without changing the gas flow rate, for instance by modifying the reactor setup and hence the flow configuration. Indeed, at a high gas velocity, there is a larger difference between GA and gas flow velocity due to some ionization downstream the arc channel, slowing down the arc movement. Additionally, the occurrence of back-breakdown events, creating new conducting arc channels, will also cause a difference between GA and gas flow velocity, so we also investigated the effect of these back-breakdown events on the calculated CO_2 conversion and energy efficiency. Our calculations clearly indicate that the back-breakdown events, which generally take place at a high gas flow rate, can help to further increase the CO_2 conversion and energy efficiency.

This study is of great interest for GA based CO_2 conversion, as we were able to elucidate the main underlying mechanisms and chemical reactions of the conversion process by means of a model that was validated by experiments. In general, we illustrated that GA based CO_2 conversion is quite promising, when compared with the classical thermal CO_2 conversion process, as well as with other plasma types. This is attributed to its non-equilibrium character, promoting the vibrational kinetics. However, we believe there is still room for improvement. Indeed, we could identify the limiting factors of the CO_2 conversion in the GA, and thus propose solutions on how to further improve the performance.

Acknowledgements

References

[1] J. Albo, M. Alvarez-Guerra, P. CastaÇo, A. Irabien, Towards the electrochemical conversion of carbon dioxide into methanol, Green Chem. 17 (2015) 2304 –2324.

[2] G. Fiorani, W. Guo, A. W. Kleij, Sustainable conversion of carbon dioxide: the advent of organocatalysis, Green Chem. 17 (2015) 1375 –1389.

[3] W. McDonough, M. Braungart, P. Anastas, J. Zimmerman, Peer reviewed: Applying the principles of green engineering to cradle-to-cradle design, Environ. Sci. Technol. 37 (2003) 434A– 441A.

[4] A. Czernichowski, Gliding arc. Applications to engineering and environment control, Pure & Appl. Chem. 66 (1994) 1301-1310.

[5] A. Indarto, D. R. Yang, J. W. Choi, H. Lee, H. K. Song, Gliding arc plasma processing of CO_2 conversion, J. Hazard. Mater. 146 (2007) 309–315.

[6] T. Nunnally, K. Gutsol, A. Rabinovich, A. Fridman, A. Gutsol, A. Kemoun, Dissociation of CO_2 in a low current gliding arc plasmatron, J. Phys. D. Appl. Phys. 44 (2011) 274009.

[7] C. S. Kalra, A. F. Gutsol, A. A. Fridman. Gliding arc discharges as a source of intermediate plasma for methane partial oxidation, IEEE Trans. Plasma Sci. 33 (2005) 32-41.

[8] T. Sreethawong, P. Thakonpatthanakun, S. Chavadej, Partial oxidation of methane with air for synthesis gas production in a multistage gliding arc discharge system, Int. J. Hydrogen Energy 32 (2007) 1067-1079.

[9] Y. N. Chun, H.O. Song, Syngas production using gliding arc plasma, Energy Sources. A: Recov. Util. Environ. Eff. 30 (2008) 1202-1212.

[10] A. Indarto, J.W .Choi, H. Lee, H.K. Song, Conversion of CO_2 by gliding arc plasma, Environ. Eng. Sci. 23(2006) 1033-1043.

[11] S. C. Kim, M. S. Lim, Y. N. Chum, Reduction characteristics of carbon dioxide using a plasmatron, Plasma Chem. Plasma Process. 34 (2014) 125-143.

[12] H. Zhang, X. D. Li, F. S. Zhu, K. F. Cen, C. M. Du, X Tu, Plasma assisted dry reforming of methanol for clean syngas production and high-efficiency CO_2 conversion, Chem. Eng. J. 310 (2017) 114-119.

[13] H. Zhang, C. M. Du, A. J. Wu, Z. Bo, J. H. Yan, X. D. Li, Rotating gliding arc assisted methane decomposition in nitrogen for hydrogen production, Int. J. Hydrogen Energy 39 (2014) 12620-12635.

[14] A. A. Fridman, S. Nester, L. A. Kennedy, A. Saveliev, O. Mutaf-Yardimci, Gliding arc gas discharge, Prog. Energy Combust. Sci. 25 (1999) 211-231.

[15] R. Burlica, M. J. Kirkpatrick, B. R. Locke, Formation of reactive species in gliding arc discharges with liquid water, J. Electrostatics 64 (2016) 35–43.

[16] B. S. Patil, J. R. Palau, V. Hessel, Jüergen Lang, Q. Wang, Plasma nitrogen oxides synthesis in a milli-scale gliding arc reactor: investigating the electrical and process parameters, Plasma Chem. Plasma Process. 36 (2016) 241–257.

[17] G. Petitpas, J. D. Rollier, A. Darmon, J. Gonzalez-Aguilar, R. Metkemeijer, L. Fulcheri, A comparative study of non-thermal plasma assisted reforming technologies, Int. J. Hydrogen Energy 32 (2007) 2848– 2867.

[18] A. Gutsol, A. Rabinovich, A. Fridman, Combustion-assisted plasma in fuel conversion, J. Phys. D: Appl. Phys. 44 (2011) 274001.

[19] A. Fridman, Plasma Chemistry, Cambridge, Cambridge University Press, 2008.

[20] X. Tu, H. J. Gallon, J. C. Whitehead, Dynamic behavior of an atmospheric argon gliding arc plasma, IEEE Trans. Plasma Sci. 39 (2011) 2900-2901.

[21] X. Tu, J. C. Whitehead, Plasma dry reforming of methane in an atmospheric pressure AC gliding arc discharge: cogeneration of syngas and carbon nanomaterials, Int. J. Hydrogen Energy 39 (2004) 9658-9669.

[22] S. Pellerin, J. M. Cormier, F. Richard, K. Musiol, J. Chapelle, Determination of electrical parameters of

bi-dimensional DC Glidarc, J. Phys. D: Appl. Phys. 32 (1999) 891–897.

[23] I. V. Kuznetsova, N. Y. Kalashnikov, A. F. Gutsol, A. A. Fridman, L. A. Kennedy, Effect of 'overshooting' in the transitional regimes of the low-current gliding arc discharge, J. Appl. Phys. 92 (2002) 4231–4237.

[24] A. Czernichowski, H. Nassar, A. Ranaivosoloarimanana, Spectral and electrical diagnostics of gliding arc, Acta Physic A Polonica A 89 (1996) 595-596.

[25] O. Mutaf-Yardimci, A. V. Saveliev, A. A. Fridman, L. A. Kennedy, Thermal and nonthermal regimes of gliding arc discharge in air flow, J. Appl. Phys. 84 (1998) 1062-1641.

[26] T. Kozák, A. Bogaerts, Splitting of CO_2 by vibrational excitation in non-equilibrium plasmas: a reaction kinetics model, Plasma Sources Sci. Technol. 23 (2014) 045004.

[27] T. Kozák, A. Bogaerts, Evaluation of the energy efficiency of CO_2 conversion in microwave discharges using a reaction kinetics model, Plasma Sources Sci. Technol. 24 (2015) 015024.

[28] R. Aerts, W. Somers, A. Bogaerts, Carbon dioxide splitting in a dielectric barrier discharge plasma: a combined experimental and computational study, ChemSusChem 8 (2015) 702-716.

[29] R. Snoeckx, R. Aerts, X. Tu, A. Bogaerts, Plasma-based dry reforming: a computational study ranging from the nanoseconds to seconds time scale, J. Phys. Chem. C 117 (2013) 4957-4970.

[30] S. Heijkers, R. Snoeckx, T. Kozák, T. Silva, T. Godfroid, N. Britun, R. Snyders, A. Bogaerts, CO_2 conversion in a microwave plasma reactor in the presence of N_2: elucidating the role of vibrational levels, J. Phys. Chem. C 119 (2015) 12815–12828.

[31] R. Snoeckx, S. Heijkers, K. Van Wesenbeeck, S. Lenaerts, A. Bogaerts, CO_2 conversion in a dielectric barrier discharge plasma: N_2 in the mix as a helping hand or problematic impurity? Energy Environ. Sci. 9 (2016) 999—1011

[32] W. Z. Wang, B. Patil, S.Heijkers, V.Hessel, and A. Bogaerts, Nitrogen fixation by gliding arc plasma: better insight by chemical kinetics modelling, ChemSusChem 10 (2017) 2145-2157.

[33] F. Richard, J. M. Cormier, S. Pellerin, J. Chapelle, Physical study of a gliding arc discharge, J. Appl. Phys. 79 (1996) 2245–2250.

[34] S. Pellerin, F. Richard, J. Chapelle, J. M. Cormier, K. Musiol, Heat string model of bi-dimensional DC Glidarc, J. Phys. D: Appl. Phys. 33 (2000) 2407-2419.

[35] St. Kolev, A. Bogaerts, A 2D model for a gliding arc discharge, Plasma Sources Sci. Technol. 24 (2015) 015025.

[36] St. Kolev, A. Bogaerts, Similarities and differences between gliding glow and gliding arc discharges, Plasma Sources Sci. Technol. 25 (2015) 035014.

[37] G. Trenchev, St. Kolev, A. Bogaerts, A 3D model of a reverse vortex flow gliding arc reactor, Plasma Sources Sci. Technol. 24 (2015) 015025.

[38] S. R. Sun, St. Kolev, H. X. Wang, A. Bogaerts, Coupled gas flow-plasma model for a gliding arc: investigations of the back-breakdown phenomenon and its effect on the gliding arc characteristics, Plasma Sources Sci. Technol. 26 (2016) 015003.

[39] St. Kolev, S.R. Sun, G. Trenchev, W. Wang, H.X. Wang and A. Bogaerts, Quasi-neutral modeling of gliding arc plasmas, *Plasma Process. Polym.* 14(2017), (in press). DOI: 10.1002/ppap.201600110.

[40] S. R. Sun, H. X. Wang, D. H. Mei, X. Tu, A. Bogaerts, CO_2 conversion in a gliding arc plasma: Performance improvement based on chemical reaction modelling, Journal of CO_2 Utilization 17 (2017) 220–234.

[41] W. Z. Wang, A. Berthelot, St. Kolev, X. Tu, A. Bogaerts, CO_2 conversion in a gliding arc plasma: 1D cylindrical discharge model, Plasma Sources Sci. Technol. 25 (2015) 065012.

[42] A. Berthelot, A. Bogaerts, Modeling of plasma-based CO_2 conversion: lumping of the vibrational levels, Plasma Sources Sci. Technol. 25 (2016) 045022.

[43] http://www.comsol.com

[44] G. J. M Hagelaar and L. C. Pitchford, Solving the Boltzmann equation to obtain electron transport coefficients and rate coefficients for fluid models, Plasma Sources Sci. Technol. 14 (2005) 722–733.

[45] S. P. Gangoli, A. F. Gutsol and A. A. Fridman, A non-equilibrium plasma source: magnetically stabilized gliding arc discharge: I. Design and diagnostics, *Plasma Sources Sci. Technol.* 19 (2010) 065003.

[46] S. P. Gangoli 2007 Design and Preliminary Characterization of the Magnetically Stabilized Gliding Arc, Master thesis, Drexel University.

[47] T. L. Zhao, Y. Xu, Y. H. Song, X. S. Li, J. L. Liu, J. B. Liu and A. M. Zhu, Determination of vibrational and rotational temperatures in a gliding arc discharge by using overlapped molecular emission spectra, J. Phys.

D: Appl. Phys. 46 (2013) 345201.

[48] A. J. Wu, J. H. Yan, H. Zhang, M. Zhang, C. M. Du, X. D. Li, Study of the dry methane reforming process using a rotating gliding arc reactor, Int. J. Hydrogen Energy 39 (2014) 17656-17670.

[49] T. Nunnally 2011 Application of Low Current Gliding Arc Plasma Discharges for Hydrogen Sulfide Decomposition and Carbon Dioxide Emission Reduction, PhD Thesis, Drexel University.

[50] J. L. Liu, H. Park, W Chung, D Park, High-Efficient conversion of CO_2 in AC-pulsed tornado gliding arc plasma, Plasma Chem. Plasma Process. 36 (2016) 437–449.

[51] M. Ramakers, G. Trenchev, S.Heijkers, W.Wang, Annemie Bogaerts, Gliding arc plasmatron: providing an alternative method for carbon dioxide conversion, Chemsuschem 10 (2017), 2642–2652.

[52] L. F. Spencer and A. D. Gallimore, CO_2 dissociation in an atmospheric pressure plasma/catalyst system: a study of efficiency, Plasma Sources Sci. Technol. 22 (2013) 15019.

[53] M. Leins, S. Gaiser, J. Kopecki, W.A. Bongers, A. Goede, M. F. Graswinckel, A. Schulz, M. Walker, M.C.M. van de Sanden and T. Hirth, 22nd International Symposium on Plasma Chemistry, P-II-8-18, Antwerp, Belgium, 2015.

[54] J. Q. Zhang, J. S. Zhang, Y. J. Yang and Q. Liu, Oxidative coupling and reforming of methane with carbon dioxide using a pulsed microwave plasma under atmospheric pressure, Energy Fuels 17 (2003) 54–59.

[55] N. Britun, T. Godfroid and R. Snyders, Time-resolved study of pulsed Ar–N_2 and Ar–N_2–H_2 microwave surfaguide discharges using optical emission spectroscopy, Plasma Sources Sci. Technol. 21 (2012) 035007.

[56] S. Paulussen, B. Verheyde, X. Tu, C. De Bie, T. Martens, D. Petrovic, A. Bogaerts and B. Sels, Conversion of carbon dioxide to value-added chemicals in atmospheric pressure dielectric barrier discharges Plasma Sources Sci. Technol.**19** (2010) 034015.

[57] R. Aerts, W. Somers and A. Bogaerts, Carbon dioxide splitting in a dielectric barrier discharge plasma: a combined experimental and computational study,ChemSusChem**8** (2015) 702–716.

[58] Q. Yu, M. Kong, T. Liu, J. Fei and X. Zheng, Characteristics of the decomposition of CO_2 in a dielectric packed-bed plasma reactor,Plasma Chem. Plasma Process. **32** (2012) 153–163.

[59] F. Brehmer, S. Welzel, M. C. M. Van De Sanden and R. Engeln, CO and byproduct formation during CO_2 reduction in dielectric barrier discharges, J. Appl. Phys. **116** (2014) 123303.

[60] D. Mei, X. Zhu, Y. He, J. D. Yan, X. Tu, Plasma-assisted conversion of CO_2 in a dielectric barrier discharge reactor: Understanding the effect of packing materials, Plasma Sources Sci. Technol. 24 (2015) 015011.

[61] X. Tu and J. C. Whitehead, Plasma-catalytic dry reforming of methane in an atmospheric dielectric barrier discharge: Understanding the synergistic effect at low temperature, Appl. Catal. B: Environ. 125 (2012) 439-448.

[62] M. S. Bak, S. K. Im and M. Cappelli, Nanosecond-pulsed discharge plasma splitting of carbon dioxide, IEEE Trans. Plasma Sci., 43 (2015) 1002–1007.

[63] M. Scapinello, L. M. Martini, G. Dilecce and P. Tosi, Conversion of CH_4/CO_2 by a. nanosecond repetitively pulsed discharge, J. Phys. D: Appl. Phys. 49 (2016) 075602.

[64] G. Horvath, J. Skalny and N. Mason, FTIR study of decomposition of carbon dioxide in DC corona discharges, J. Phys. D: Appl. Phys. 41 (2008) 225207.

[65] A. Lebouvier, S. A. Iwarere, P.d'Argenlieu, D. Ramjugernath and L. Fulcheri, Assessment of carbon dioxide dissociation as a new route for syngas production: a comparative review and potential of plasma-based technologies, Energy Fuels 27 (2013) 2712–2722.

[66] O. Taylan and H. Berberoglu, Dissociation of carbon dioxide using a microhollow cathode discharge plasma reactor: effects of applied voltage, flow rate and concentration, Plasma Sources Sci. Technol. 24 (2015) 015006.

[67] P. J. Lindner, S. Y. Hwang and R. S. Besser, Analysis of a microplasma fuel reformer with a carbon dioxide decomposition reaction, Energy Fuels 27 (2013) 4432–4440.

[68] B. Zhu, X. S. Li, J. L. Liu, X. Zhu and A. M. Zhu, Kinetics study on carbon dioxide reforming of methane in kilohertz spark-discharge plasma, Chem. Eng. J. 264 (2015) 445-452.

[69] V. D. Rusanov, A. a. Fridman and G. V. Sholin, The physics of a chemically active plasma with nonequilibrium vibrational excitation of molecules,Sov. Phys. Usp. 24 (1981) 447–474.

[70] R. I. Asisov, A. K. Vakar, V. K. Jivotov, M. F. Krotov, O. A. Zinoviev, B. V Potapkin, A. A. Rusanov, V. D. Rusanov and A. A. Fridman, Non-equilibrium plasma-chemical CO_2 dissociation in supersonic flow, Proc.

USSR Acad. Sci. (1983) 271.

[71] W. Bongers, H. Bouwmeester, B. Wolf, F. Peeters, S. Welzel, D. van den Bekerom, N. den Harder, A. Goede, M. Graswinckel, P. W. Groen, J. Kopecki, M. Leins, G. van Rooij, A. Schulz, M. Walker and R. van de Sanden, Plasma-driven dissociation of CO_2 for fuel synthesis, Plasma Process. Polym., 2016 DOI: 10.1002/ppap.201600126.

[72] A. Bogaerts, T. Kozák, K. Van Laer and R. Snoeckx, Plasma-based conversion of CO_2: current status and future challenges, Faraday Discuss. 183 (2015) 217-232

[73] A. Berthelot, A. Bogaerts, Modeling of CO_2 Splitting in a Microwave Plasma: How to Improve the Conversion and Energy Efficiency, J. Phys. Chem. C, 2017, in press.

[74] Y. Tagawa, S. Mori, M. Suzuki, I. Yamanaka, T. Obara, J. Ryu and Y. Kato, Synergistic decomposition of CO_2 by hybridization of a dielectric barrier discharge reactor and a solid oxide electrolyser cell, KAGAKU KOGAKU RONBUNSHU 37 (2011) 114–119.

[75] R. Aerts, R. Snoeckx, A. Bogaerts, In-Situ chemical trapping of oxygen in the splitting of carbon dioxide by plasma, Plasma Processes Polym. 11 (2014) 985– 992.

[76] Y. C. Kim and M. Boudart, Recombination of oxygen, nitrogen, and hydrogen atoms on silica: kinetics and mechanism, Langmuir 7 (1991) 2999–3005.

[77] J. Adanez, A. Abad, F. Garcia-Labiano, P. Gayan and L. F. de Diego, Progress in Chemicals-looping combustión and reforming technologies, Prog. Energy Combust. Sci. 38 (2012) 215–282.

[78] M. M. Hossain and H. I. de Lasa, Chemical-looping combustion (CLC) for inherent CO_2 separations-a review, Chem. Eng. Sci. 63 (2008) 4433–4451.

[79] S. Mori, N. Matsuura, L. L. Tun and M. Suzuki, Direct synthesis of carbon nanotubes from only co_2 by a hybrid reactor of dielectric barrier discharge and solid oxide electrolyser cell, Plasma Chem. Plasma Process. 36 (2016) 231–239.

[80] S. Mori, N. Matsuura and L. L. Tun, Synergistic CO_2 conversion by hybridization of dielectric barrier discharge and solid oxide electrolyser cell, Plasma Process. Polym. 9999 (2016) 1–6.

[81] Z. Bo, Fundamental research of the treatment of volatile organic compounds with gliding arc discharge plasma, PhD thesis, 2008, Zhejiang University, Hangzhou, China.

[82] S. H. Hu, Methane conversion using gliding arc discharge plasma, PhD thesis, 2012, Tianjin University, Tianjin, China.

[83] Z. Bo, J. H. Yan, X. Li, Y. Ch, K. F. Cen, Scale-up analysis and development of gliding arc discharge facility for volatile organic compounds decomposition, 155 (2008) 494–501.

[84] S. Pellerin, O. Martinie, J. M. Cormier, J. Chapelle and P. Lefaucheux, Back-breakdown phenomenon in low current discharge at atmospheric pressure in transversal flow, High Temp. Mater. Process. 2 (1999) 167–180.

[85] W. Z. Wang, A. Bogaerts, Effective ionisation coefficients and critical breakdown electric field of CO_2 at elevated temperature: effect of excited states and ion kinetics, Plasma Sources Sci. Technol. 25 (2015) 055025.